Bod1l is required to suppress deleterious resection of stressed replication forks

Higgs, Martin; Reynolds, John; Winczura, Alicja; Blackford, AN; Borel, Valerie; Miller, Edward; Zlatanou, Anastasia; Nieminuszczy, Jadwiga; Ryan, Ellis; Davies, Nicholas; Stankovic, Tatjana; Boulton, Simon; Niedzwiedz, Wojciech; Stewart, Grant

Document Version
Early version, also known as pre-print

[Link to publication on Research at Birmingham portal](#)

1 **BOD1L IS REQUIRED TO SUPPRESS DELETERIOUS RESECTION OF STRESSED**

2 **REPLICATION FORKS**

3

4 Martin R. Higgs[1,4], John J. Reynolds[1,4], Alicja Winczura[2¤], Andrew N. Blackford[2§], Valérie Borel[3],

5 Edward S. Miller[1¤], Anastasia Zlatanou[1], Jadwiga Nieminuszczy[2], Ellis L. Ryan[1], Nicholas J.

6 Davies[1], Tatjana Stankovic[1], Simon J. Boulton[3], Wojciech Niedzwiedz[2], Grant S. Stewart[1*].

7

8 [1] School of Cancer Sciences, University of Birmingham, Birmingham, B15 2TT, UK

9 [2] The Weatherall Institute of Molecular Medicine, University of Oxford, Oxford, OX3 9DS, UK.

10 [3] London Research Institute, Clare Hall Laboratories, South Mimms, Herts, EN6 3LD, UK.

11 [4] Co-first author.

12

13 [*] Correspondence: g.s.stewart@bham.ac.uk

14 [§] Current address: Wellcome Trust/Cancer Research UK Gurdon Institute, University of

15 Cambridge, Cambridge, CB2 1QN, UK.

16 [¤] Current address: Division of Biomedical Cell Biology, The University of Warwick, Coventry, CV4

17 7AL, UK.

18

19 **RUNNING TITLE:** BOD1L prevents DNA-2 dependent fork resection

20

21 **CHARACTER COUNT:** 59,966

22

SUMMARY

Recognition and repair of damaged replication forks is essential to maintain genome stability, and is coordinated by the combined action of the Fanconi Anaemia and homologous recombination pathways. These pathways are vital to protect stalled replication forks from uncontrolled nucleolytic activity, which otherwise causes irreparable genomic damage. Here we identify BOD1L as a component of this fork protection pathway, which safeguards genome stability after replication stress. Loss of BOD1L confers exquisite cellular sensitivity to replication stress and uncontrolled resection of damaged replication forks, due to a failure to stabilise Rad51 at these forks. Blocking DNA2-dependent resection, or down regulation of the helicases BLM and Fbh1, suppresses both catastrophic fork processing and the accumulation of chromosomal damage in BOD1L-deficient cells. Thus, our work implicates BOD1L as a critical regulator of genome integrity that restrains nucleolytic degradation of damaged replication forks.

INTRODUCTION

Replication stress is any pathological process that compromises the fidelity of genome duplication (Zeman and Cimprich, 2014). The Fanconi Anaemia (FA)/homologous recombination (HR) pathway plays a central role in combatting replication stress (Gari and Constantinou, 2009). FA is a rare chromosomal instability syndrome characterized by severe developmental abnormalities, tumour predisposition and a hypersensitivity to agents that induce DNA inter-strand cross-links (ICLs), such as mitomycin C (MMC) and cisplatin. To date, mutations in at least 16 different genes (FA complementation groups A-Q) have been identified in patients exhibiting features consistent with FA (reviewed in Walden and Deans, 2014).

Whilst historically the FA/HR pathway has been associated with the HR-dependent repair of ICLs, it plays a broader role in protecting cells from replication stress. Indeed, HR-deficient (and some FA) cell lines are hypersensitive to replication stress-inducing agents that do not induce ICLs (e.g. aphidicolin [APH] and hydroxyurea [HU]) (Howlett *et al.*, 2005). It has been proposed that FA and HR proteins function to: (i) protect stalled/collapsed forks from uncontrolled nucleolytic attack (which may render such forks unrecoverable and/or prone to inappropriate repair) (Schlacher *et al.*, 2011; 2012); and (ii) in some cases may facilitate their restart once repair is complete. Cells defective in these processes exhibit an increase in under-replicated DNA, particularly at common fragile sites (CFS). This can result in the generation of ultra-fine anaphase bridges (UFBs), and can ultimately manifest as chromosome breakage and micronuclei (Naim and Roselli, 2009a). The accumulation of such genetic damage over time eventually triggers cell death, and may contribute to the attrition of highly replicating cells, such as germ and haematopoietic cells (Garaycoechea and Patel, 2014).

Despite extensive research, it is still not completely understood how the cell regulates repair of replication damage via the FA/HR pathway. A wide variety of DNA damage response (DDR) and DNA repair proteins, including components of the FA/HR pathway, are recruited to stalled forks upon replication stress (Sirbu *et al.*, 2013). However, it is unclear how replication forks requiring repair are marked: this might involve RPA coated ssDNA, specific DNA secondary structures or damage-inducible post-translational modifications of the replication machinery and/or

63 surrounding chromatin. It is also likely that some repair proteins are constitutive components of the

64 replication fork machinery, to allow immediate initiation of the DDR once a lesion is encountered.

65   We have identified an uncharacterised factor, BOD1L, associated with newly replicated

66 chromatin. Cells lacking BOD1L accumulate catastrophic levels of genome damage following

67 replication stress, particularly after MMC exposure, manifesting as excessive chromosome

68 breakage. Although related to the mitotic regulator BOD1, we demonstrate that BOD1L does not

69 regulate spindle orientation but rather functions to protect stalled/damaged replication forks from

70 uncontrolled DNA2-dependent resection. We further show that BOD1L functions within the FA

71 pathway as part of the fork protection machinery, to stabilize Rad51 on chromatin by suppressing

72 the anti-recombinogenic and pro-resection activities of Fbh1 and BLM. Taken together, our data

73 establish that BOD1L is a critical factor associated with the replication machinery that acts to

74 promote fork stability by counteracting negative regulators of HR.

75

RESULTS

BOD1L is an uncharacterised factor that maintains genome stability following replication stress

Isolation of proteins on nascent DNA (iPOND) is a robust method for the detection of proteins at sites of newly replicated DNA (Sirbu *et al.,* 2013). However, many proteins are sensitive to the harsh conditions of iPOND. To overcome this issue, we first modified the original iPOND protocol and subsequently utilised this new method coupled with mass spectrometry to identify factors associated with nascent chromatin. As with other iPOND-based proteomic studies (Sirbu *et al.*, 2013), we identified numerous replication machinery components at ongoing forks, including the MCM helicase, PCNA, the RFC complex, RPA and the replicative polymerases, polδ and polα (**Figure S1A**). In addition to these proteins, we also identified Biorientation Defect 1-like (BOD1L); a large, previously uncharacterised protein with N-terminal homology to the mitotic regulator BOD1 (**Figure 1A**) (Porter *et al*, 2007). Consistent with these data, we confirmed the presence of BOD1L in EdU precipitates by Western blotting (**Figure 1B**). To verify that BOD1L associated with replication fork proteins, we performed proximity-ligation assays with antibodies against PCNA and BOD1L. We readily detected nuclear PLA signals in undamaged EdU-positive cells, which were strongly reduced in EdU-negative and BOD1L-depleted cells (**Figures 1C-D**). Moreover, we could co-immunoprecipitate BOD1L, and murine GFP-tagged Bod1l, with Mcm2 and Mcm7 (**Figures 1E and S1B**). Together, these data indicate that BOD1L is localised at/near replication forks.

In addition to its homology to BOD1, the amino acid sequence of BOD1L also contains several *in vivo* ATM/ATR phosphorylation sites (Matsuoka *et al.* (2007)), suggesting that BOD1L might play a role in the DDR. To investigate this, we depleted cells of BOD1L using siRNA and analysed cellular sensitivity to a range of DNA damaging agents. Knockdown of BOD1L exquisitely hypersensitised cells to agents that induce replicative stress, in particular MMC (**Figures 1F and S1C**), and was significantly more severe than loss of FANCA. However, co-depletion of FANCA and BOD1L revealed that these two factors were epistatic for MMC hypersensitivity, suggesting that BOD1L may function within the FA pathway. Treatment of BOD1L-depleted cells with replication stress-inducing agents also induced increased micronuclei formation, indicating a critical role for BOD1L in maintaining genome stability upon replication damage (**Figure 1G**).

105   Importantly, these observations were recapitulated in several cell lines, and in two independent

106   DT40 BOD1L knockout clones (**Figures S1D-H**), demonstrating that the genome instability

107   observed is specifically due to loss of BOD1L, and is neither cell line nor organism specific.

108

109   **BOD1L and BOD1 are functionally distinct**

110   BOD1 is a mitotic factor that associates with metaphase chromosomes and is essential for

111   correct orientation of the mitotic spindle (Porter *et al*, 2007; Porter *et al*, 2013). Given the sequence

112   similarity of the N-terminus of BOD1L to BOD1, it was conceivable that the increased micronuclei

113   observed in BOD1L-depleted cells arose from mitotic abnormalities.

114   To first investigate whether BOD1L was functionally related to BOD1, we performed

115   phenotypic analyses of cells depleted of either BOD1 or BOD1L by siRNA. Whilst loss of BOD1L

116   resulted in elevated DDR signalling, specifically the phosphorylation of H2AX and RPA2, this

117   defect was not observed in BOD1-depleted cells (**Figure 2A**). Furthermore, loss of BOD1 neither

118   increased MMC-induced micronuclei, nor engendered a cellular hypersensitivity to MMC or HU

119   (**Figures 2B-D**). In addition, unlike BOD1 depletion, loss of BOD1L did not cause mitotic or spindle

120   alignment defects (**Figures 2E-F**). Finally, immunostaining analyses of MMC-treated cells revealed

121   that BOD1L depletion increases the proportion of micronuclei that are acentric (CENPA-negative)

122   and that contain DNA double strand breaks (DSBs) (53BP1-positive), suggesting that these

123   micronuclei originated from unrepaired DNA damage (**Figure 3A**). Together, these observations

124   demonstrate that BOD1 and BOD1L perform separate roles in cell cycle regulation and genome

125   maintenance respectively.

126

127   **BOD1L functions within the Fanconi Anaemia pathway**

128   Micronuclei are observed in the absence of several genome stability factors, although FA-

129   deficient are especially prone to ICL-induced micronucleation (Naim and Rosselli, 2009a). It has

130   been proposed that micronuclei arising in cells undergoing replication stress stem from a failure to

131   complete timely DNA replication. This results in the persistence of under-replicated DNA in cells as

132   they enter mitosis, which can manifest as UFBs, typically marked by PICH and flanked by

133   FANCD2 foci (Chan *et al.,* 2007; Chan *et al.,* 2009). These can lead to chromosome breakage and

6

134 packaging of the damaged DNA into 53BP1 bodies visible in the subsequent G1 phase (Lukas *et*

135 *al.*, 2011).

136   We next determined the prevalence of late replicating DNA, UFBs and G1-phase 53BP1

137 bodies in BOD1L deficient cells following MMC exposure. Loss of BOD1L dramatically increased

138 the percentage of mitotic cells positive for either FANCD2/PICH positive UFBs or for EdU foci

139 following MMC exposure (**Figures 3B-D**). Consistent with this, we observed a significant rise in the

140 number of 53BP1 G1 bodies in these cells, which was again more severe than depletion of FANCA

141 alone (**Figures 3E-F**). Collectively, these data suggest that the micronuclei observed in BOD1L-

142 deficient cells are due to a failure to correctly resolve replication stress.

143   FA cells exhibit chromosomal hypersensitivity to agents that induce ICLs, caused in part by

144 the presence of under-replicated DNA, and exhibit chromatid breakage at specific loci, namely

145 CFS (Barlow *et al.*, 2013; Durkin *et al.,* 2007; Schoder *et al.*, 2010). Strikingly, loss of BOD1L

146 resulted in catastrophic levels of chromosome breakage following MMC exposure, which was

147 markedly more severe than FANCA loss (**Figures 3G and S2A**). In agreement with previous data,

148 co-depletion of FANCA/BOD1L had no additional effect on genome instability. Furthermore, the

149 majority of BOD1L-deficient cells showed evidence of chromosome breakage at the CFS locus

150 FRA16D (**Figure 3H**). Importantly, genome stability in BOD1L-depleted cells was restored by the

151 stable expression of murine Bod1L, which is resistant to siRNA-mediated degradation, in two

152 independent HeLa cell clones (CFlap-mBod1L C1-4 and C5-20) (**Figures S2B-D**). Taken together,

153 these observations clearly demonstrate that BOD1L functions to resolve replication stress, in

154 conjunction with FA pathway components (Naim and Rosselli, 2009b).

155   Given that BOD1L is epistatic with a core FA pathway component, we evaluated the

156 functional integrity of this pathway in the absence of BOD1L. The DNA damage-induced mono-

157 ubiquitylation of FANCD2 is a central event within the FA pathway, and is often used as a marker

158 of FA pathway integrity (Smogorzewska *et al.*, 2007). Loss of BOD1L had no effect on the focal

159 recruitment of FANCD2 to sites of MMC damage, nor its ability to be mono-ubiquitylated (**Figures**

160 **S2E-F**), suggesting that BOD1L functions downstream of the FA core and FANCI/D2 complexes

161 within the FA/HR pathway.

162

BOD1L depletion compromises the fidelity of DNA replication following replication stress

The cellular response to replication stress is primarily coordinated by the ATR kinase, which activates the intra-S phase checkpoint and protects stalled replication forks from collapse. Recent studies on ATR-deficient cells have demonstrated that fork protection is crucial to maintain CFS integrity (Koundrioukoff et al., 2013). Given that BOD1L-depleted cells exhibit CFS instability, this suggests that BOD1L may protect replication forks directly, in a similar fashion to ATR. We therefore hypothesised that loss of BOD1L would negatively impact S-phase regulation and/or replication fork dynamics upon replication stress.

Initially, we sought to determine the effect of depleting BOD1L on cell cycle progression. Compromising BOD1L expression had little effect on cell cycle progression in the absence of DNA damage (**Figure 4A**). However, consistent with a defect in resolving S-phase damage, cells lacking BOD1L rapidly accumulated in G2-phase following MMC exposure, with a concomitant reduction in mitotic index (**Figures 4B and S3A-B**); a phenotype reminiscent of FA cells (Akkari *et al.*, 2001; Heinrich *et al.*, 1998;). Next, to directly analyse the stability of on-going replication forks following HU treatment, we quantified the symmetry of sister replication forks originating from the same origin and travelling in opposite directions. Since sister forks typically display similar replication rates (Conti *et al.*, 2007), marked fork asymmetry indicates that individual forks are more prone to stalling (Rodriguez-Lopez *et al.,* 2002). Supportive of a role for BOD1L in promoting fork stability, we observed a significant increase in replication fork asymmetry in BOD1L depleted cells following HU treatment (**Figure 4C**), suggesting that damaged forks are slower to restart and/or are more susceptible to stalling in its absence.

We also observed a significant increase in new origin firing in response to both HU and MMC in cells lacking BOD1L, which was dependent on Cdk1/2 activity (**Figures 4D-E and S3C-E**). However, this origin firing was not due to defective ATR/Chk1 signalling, since BOD1L-depleted cells were proficient for Chk1 phosphorylation on both S317 and S345 in response to MMC (**Figure 4F**). This phenotype was also not present in cells depleted of BOD1, further strengthening the functional divergence of these proteins (**Figure S3F**).

Despite observing increased new origin firing and replication fork asymmetry in BOD1L depleted cells after replication stress, there was no concomitant reduction in the number of

8

192 restarted forks, nor any increase in fork stalling (first label terminations). One possible explanation

193 was that new origins were firing proximal to stalled/collapsed (red only labelled) forks in BOD1L

194 depleted cells, therefore artificially enhancing the quantification of restarted (red and green

195 labelled) replication forks. To investigate this, we used a Cdk1/2 inhibitor to inhibit new origin firing

196 in cells lacking BOD1L, and examined the impact on fork stalling/restart. Accordingly, we found

197 that inhibition of Cdk1/2 activity during HU exposure ablated new origin firing, increased the

198 prevalence of stalled replication forks, and decreased fork restart (**Figure S3G**), suggesting that

199 BOD1L prevents fork stalling upon replication stress.

200   Together, these data suggest that, upon the induction of replication stress, a lack of BOD1L

201 compromises fork stability and/or restart, which triggers dormant origin firing proximal to the

202 stalled/damaged fork.

203

204 **BOD1L protects stalled forks from uncontrolled resection**

205   It is thought that uncontrolled origin firing in the absence of ATR leads to excessive ssDNA

206 generation and exhaustion of cellular pools of RPA, which both cause irreversible fork collapse

207 (Toledo *et al.*, 2013). It is conceivable that global depletion of soluble RPA may also underlie the

208 excessive chromosome breakage observed in BOD1L deficient cells, since they also exhibit

209 increased origin firing, fork instability and defective fork restart. To investigate this, we first sought

210 to determine levels of ssDNA present in BOD1L-depleted cells following MMC exposure. Loss of

211 BOD1L resulted in a significant increase in RPA loading onto damaged chromatin compared to

212 control cells (**Figures 5A-B and S4A**). Moreover, ablation of BOD1L expression significantly

213 enhanced the formation of MMC-induced native BrdU foci (**Figures 5C and S4B**), consistent with

214 increased ssDNA generation in these cells. However, in contrast to ATR-deficient cells (Toledo *et*

215 *al.*, 2013), RPA over-expression had no effect on either new origin firing or chromosomal instability

216 in the absence of BOD1L (**Figures S4C-E**). In addition, it is clear that the ATR-Chk1 pathway is

217 functional in BOD1L deficient cells (see **Figure 4F**). Therefore, although cells lacking ATR or

218 BOD1L display phenotypic similarities, it appears that the mechanisms underlying replication fork

219 stalling/collapse differ.

220   It has been demonstrated that loss of FA pathway components such as BRCA2 and

221   FANCD2 leads to nucleolytic degradation of stalled replication forks, rendering them non-

222   permissive for repair by HR (Schlacher *et al.*, 2011; 2012). This excessive fork resection underlies

223   the increased chromosome breakage exhibited by BRCA2-null cells. The nucleases Mre11 and/or

224   DNA2 appear to perform this uncontrolled resection; inhibition of Mre11 can alleviate fork

225   degradation in BRCA2 deficient cells (Schlacher *et al.*, 2011), and depletion of DNA2 rescues the

226   hypersensitivity of FANCD2 deficient cells to cisplatin (Karanja *et al.*, 2014). To investigate whether

227   similar mechanisms underlie the phenotypes of BOD1L-deficient cells, we examined levels of

228   MMC-induced RPA2 phosphorylation on S4/S8, a well-established marker of DNA resection.

229   Depletion of BOD1L (but not BOD1) resulted in elevated levels of RPA2-S4/8 phosphorylation

230   following MMC treatment (**Figures 5D-F and 2A**), which could be restored to control levels by the

231   expression of CFlap-mBod1L (**Figure S4F**). Hyper-phosphorylation of RPA2 was also observed in

232   BOD1L-deficient cells following exposure to HU, indicating that this defect is not restricted to MMC-

233   induced ICLs (**Figure S4G**). Therefore, these data suggest that BOD1L functions to suppress

234   resection. Consistent with this, we observed an increased localisation of BOD1L to damaged forks

235   undergoing resection (**Figure 5G**).

236   To confirm that uncontrolled resection in BOD1L depleted cells occurs specifically at

237   replication forks, we used the approach described by Schlacher *et al.* (2011) to monitor

238   degradation of nascent DNA. In line with previous observations, loss of BRCA1 or BRCA2

239   increased the degradation of newly synthesized DNA at forks (apparent as a decreased IdU:CldU

240   ratio; **Figure 6A and S5A-B**). Interestingly, cells lacking BOD1L exhibited similar degradation of

241   stalled replication forks. Critically, this was epistatic with either BRCA1 or BRCA2 depletion,

242   suggesting that BOD1L and BRCA1/2 function within the same pathway to protect replication forks.

243   In support, BRCA2 and BOD1L co-depletion had no additional effect on cellular hypersensitivity to

244   MMC or RPA2 hyper-phosphorylation compared to loss of the individual genes alone (**Figure S5C-**

245   **E**). Finally, BOD1L co-immunoprecipitated with the fork protection factors FANCD2 and BRCA2

246   (**Figure 6B**). Together, this provides strong evidence that BOD1L plays a vital role in preventing

247   unconstrained resection at stalled forks, in concert with FANCD2 and BRCA1/2.

248   We next sought to ascertain whether the increased resection seen in cells devoid of

249   BOD1L was mediated by Mre11, DNA2 and/or Exo1; three nucleases implicated in fork resection.

250   In line with the study by Karanja *et al.* (2014), co-depletion of DNA2, but not Exo1, completely

251   repressed MMC-induced RPA2 S4/8 hyper-phosphorylation observed in cells lacking BOD1L

252   (**Figures S5F-G**). Furthermore, the over-resection of stalled forks was completely abolished by co-

253   depletion of DNA2 with BOD1L. However, in contrast to previous findings with BRCA1/2 and

254   FANCD2 (Schlacher *et al.*, 2011), inhibition of Mre11 by Mirin was unable to rescue nucleolytic fork

255   degradation in the absence of BOD1L (**Figures 6C and S5H**). Moreover, the combined loss of

256   DNA2 and BOD1L restored the MMC-induced micronuclei and chromosome damage to normal

257   levels (**Figure 6D-E**). This demonstrates that the severe genome instability in cells lacking BOD1L

258   arises from uncontrolled DNA2-dependent resection of damaged forks.

259

260   **BOD1L stabilises Rad51 at damaged replication forks by suppressing anti-recombinogenic**

261   **pathways**

262   The strand exchange protein Rad51 is best known as a principal effector of HR, but it also

263   plays a central role in stabilising/promoting the restart of damaged replication forks (Petermann *et*

264   *al.*, 2010; Costanzo, 2011). Accordingly, the excessive fork degradation observed in BRCA2 or

265   FANCD2 deficient cells is restored by overexpressing an ATPase-dead Rad51 mutant, which

266   stabilises Rad51 nucleofilaments on ssDNA by preventing its ATP-dependent dissociation

267   (Schlacher *et al.*, 2011; 2012). Thus, the loading of Rad51 onto stalled forks prevents uncontrolled

268   nucleolytic activity.

269   To investigate whether a defect with Rad51 function underlies the excessive fork resection

270   observed in the absence of BOD1L, we exposed BOD1L-depleted cells to MMC, and then

271   monitored the accumulation/retention of Rad51 at sites of damage by immunofluorescence.

272   Notably, MMC-induced Rad51 foci formation was severely compromised in BOD1L-depleted cells

273   (**Figure 6F**). This was observed with 4 different BOD1L siRNA sequences, and was not due to any

274   alteration in Rad51 protein expression (**Figures S5I-J**). Moreover, the defective focal recruitment

275   of Rad51 (**Figure S6A**) upon damage could be restored by the expression of CFlap-mBod1L

276   (**Figures S6B-C**). In keeping, Rad51 also failed to load efficiently onto MMC-damaged chromatin

277 in cells lacking BOD1L (**Figure 6G**). Consistent with this, BOD1L-depleted cells exhibited

278 increased numbers of MMC-induced radial chromosomes, and a concomitant decrease in the

279 frequency of MMC-induced SCEs (**Figures S6D-E**). Strikingly, the formation of IR-induced Rad51

280 foci at DSBs was unaffected in BOD1L-depleted cells (**Figure S6F**), suggesting that our

281 observations were not due to a global defect in Rad51 loading *per se*, but rather an inability to

282 localise/stabilise Rad51 to stalled replication forks.

283 Conceivably, a defect in recruiting Rad51 to stalled forks may be due to either a failure to

284 properly load Rad51 onto ssDNA, or an inability to maintain loaded Rad51 on chromatin. To

285 investigate the former possibility, we examined the impact of BOD1L depletion on the recruitment

286 of BRCA1, BRCA2 and PALB2, which are essential for Rad51 loading to ICLs (Bhattacharyya *et*

287 *al.*, 2000; Godthelp *et al.*, 2006; Xia *et al.*, 2007). Cells lacking BOD1L exhibited no observable

288 defects in the re-localisation of BRCA1, BRCA2 or GFP-PALB2 to foci following exposure to MMC

289 (**Figures 6H** and **S6G-I**), suggesting that BOD1L may instead be required to stabilise/retain Rad51

290 on damaged chromatin.

291 Proteins involved in Rad51 filament dissolution play a vital role in controlling HR and

292 maintaining genome stability. Of these, the RecQ-like helicases BLM and RECQL5, and the F-box-

293 containing helicase Fbh1 are the best studied: all three suppress Rad51-dependent HR,

294 particularly in response to replication stress. We speculated that the phenotypes observed in

295 BOD1L-deficient cells following MMC exposure may arise from the uncontrolled activity of one or

296 more of these anti-recombinase(s). We therefore siRNA-depleted BOD1L in combination with

297 BLM, Fbh1 or RECQL5, and monitored the levels of MMC-induced RPA S4/S8 phosphorylation

298 and Rad51 foci formation. Strikingly, loss of either Fbh1 or BLM (but not RECQL5) reduced MMC-

299 induced RPA S4/S8 phosphorylation and restored Rad51 focus formation in BOD1L-depleted cells

300 (**Figures 7A-B and S7A-C**). Consistent with this, co-depletion of Fbh1 in BOD1L-depleted cells

301 restored MMC-induced loading of Rad51 onto chromatin (**Figure S7D**). However, depletion of

302 Fbh1 or BLM was unable to restore Rad51 focus formation in the absence of BRCA2, suggesting

303 that BOD1L acts downstream of BRCA2 to control Rad51 (**Figure S7E**). Depleting Fbh1 or BLM

304 expression also partially alleviated the over-resection of stalled replication forks observed in cells

305 lacking BOD1L, in keeping with the notion that Rad51 suppresses aberrant fork resection.

12

306   Strikingly, RECQL5 depletion further increased fork resection in the absence of BOD1L, indicating

307   that these two factors act in separate pathways (**Figures 7C and S7F**). Lastly, ablating Fbh1 or

308   BLM expression also restored genome stability in cells depleted of BOD1L (**Figures 7D and S7G**).

309   Loss of RECQL5, however, had no restorative impact on MMC-induced chromosomal instability.

310   Finally, and in keeping with a role for BOD1L in stabilising Rad51 by counteracting BLM, both BLM

311   and Rad51 could be co-immunoprecipitated with BOD1L or CFlap-mBod1L (**Figure 7E and S7H**).

312   Taken together, these data demonstrate that BOD1L functions to restrain the pro-resection

313   and anti-recombinogenic functions of BLM/Fbh1 towards Rad51, thereby stabilising Rad51 on

314   chromatin and promoting HR-dependent repair of damaged replication forks. In the absence of

315   BOD1L, damaged replication forks undergo deleterious DNA2-dependent nucleolytic resection,

316   which compromises fork repair/restart and leads to catastrophic genome instability (**Figure 7F**).

13

DISCUSSION

The ability to efficiently resolve replication stress is vital to maintain genome stability. In this study, we have identified BOD1L as a factor associated with newly replicated chromatin that functions to prevent catastrophic DNA damage induced by replication stress by protecting damaged replication forks from promiscuous nucleolytic degradation.

Loss of Rad51-mediated fork protection underlies uncontrolled fork resection and genome instability in BOD1L deficient cells

Rad51-dependent HR plays an essential role to stabilise, protect and promote the restart of stalled or damaged replication forks. Central to this process is the BRCA1/BRCA2/PALB2-dependent loading of Rad51 onto RPA-coated ssDNA generated at such forks (Costanzo, 2011). Rad51 fork loading stabilises replication fork intermediates and prevents deleterious nucleolytic processing (Petermann *et al.*, 2010; Schlacher *et al.*, 2011; 2012). Loss of this protective activity cripples the repair/restart of damaged forks and compromises genomic integrity.

We observed that BOD1L depleted cells exhibit increased fork degradation in a manner comparable to BRCA1/BRCA2 deficient cells. This suggests that defects in the recruitment and/or stabilisation of Rad51 allow degradation of damaged forks in BOD1L-deficient cells. Yet, in marked contrast to the complete loss of BRCA2 or PALB2 (Yuan *et al.,* 1999; Xia *et al.,* 2006; Zhang *et al.,* 2009), loss of BOD1L does not impact on the recruitment of Rad51 to DSBs induced by IR. This implies that the function of BOD1L in regulating Rad51 in response to genotoxic damage is restricted to lesions that cause replication stress.

The repair and restart of forks requires the tightly regulated processing of replication damage (such as ICLs) by several different nucleases. Whilst such nucleolytic processing is important for cell survival, uncontrolled activity of these nucleases is also detrimental to genomic integrity (Adamo *et al*., 2010; Karanja *et al*., 2014). In keeping with this, uncontrolled resection of damaged forks and increased genomic instability observed in the absence of BOD1L was completely alleviated by co-depletion of DNA2. In contrast, inhibition of Mre11 activity with Mirin had no effect on the degradation of stalled replication forks in the absence of BOD1L. Since both BRCA2 and FANCD2 suppress the activity of Mre11 at stalled forks (Schlacher *et al.*, 2011; 2012;

14

346 Ying *et al.,* 2012), our data suggests that BOD1L acts independently to inhibit aberrant DNA2

347 activity. Based on this, loss of BOD1L and BRCA2 should further increase fork resection, rather

348 than exhibit the epistatic relationship we observed. Although the underlying reason is unclear, we

349 postulate that nucleolytic degradation of a damaged fork by one nuclease prohibits further

350 processing by other nucleases.

351   Interestingly, since BOD1L co-immunoprecipitated with both BRCA2 and FANCD2 in

352 unperturbed cells, this raises two intriguing possibilities: that multiple fork protection factors act to

353 individually block the activities of different nucleases towards replication forks, and that they may

354 exist in a single complex.

355

356 **Mechanisms for BOD1L in stabilising Rad51 on damaged chromatin**

357   Our data demonstrates that loss of BOD1L is epistatic with deficiencies in BRCA1/BRCA2,

358 although the phenotypes observed in the absence of BOD1L cannot be explained by an inability to

359 recruit BRCA1, BRCA2 or PALB2 to sites of replication stress. Instead, co-depletion of BOD1L with

360 the anti-recombinogenic helicases Fbh1 or BLM restored Rad51 focal recruitment, stalled

361 replication fork resection and genome stability. Thus, chromatin-bound Rad51 may be more

362 susceptible to anti-recombinases, and/or Rad51 nucleofilaments may be more unstable, in the

363 absence of BOD1L. Importantly, Fbh1 or BLM knockdown failed to recover MMC-induced Rad51

364 foci formation in BRCA2-depleted cells, suggesting that BOD1L acts downstream of

365 BRCA2/PALB2 (see **Figure S6F**). Moreover, BOD1L associates with Rad51, suggesting that it

366 may stabilise Rad51 directly. Together, our data suggest that BRCA2 and BOD1L function

367 independently in a common pathway to protect replication forks, and that BOD1L acts in a similar

368 manner to the C-terminus of BRCA2 (Esashi *et al*., 2007; Schlacher *et al*., 2011), i.e. promoting

369 Rad51 nucleofilament stability. Intriguingly, co-depletion of BOD1L with another anti-

370 recombinogenic helicase, RECQL5, failed to restore Rad51 foci formation, and actually

371 increased/accelerated fork degradation. This is in line with recent data demonstrating that the

372 combined loss of FA proteins with RECQL5 is additive in terms of fork degradation, and that BLM

373 and RECQL5 have divergent functions in the absence of an intact FA pathway (Kim *et al*., 2015).

15

374   It is unclear why depletion of two independent factors (namely BLM or Fbh1) is able to

375   compensate for a lack of BOD1L, although BLM and Fbh1 have partially redundant functions in

376   DT40 cells (Kohzaki *et al.*, 2007). Whilst Fbh1 and BLM both have pro- and anti-recombinogenic

377   activities (Bugreev *et al.*, 2007; Fugger *et al.*, 2009), BLM can displace Rad51 from ssDNA, and

378   can also potentiate HR through its ability to stimulate DNA2-dependent end-resection by binding to

379   RPA (Chen *et al.*, 2013; Xue et al., 2013; Sturrzenegger *et al.,* 2014). It is possible that loss of

380   BLM activity in BOD1L/BLM knockdown cells has two effects: (1) increases Rad51 filament

381   stability and; (2) compromises DNA2-dependent resection of damaged forks, the latter of which

382   causes the genome instability apparent in BOD1L deficient cells.

383   Currently it is unknown whether BOD1L influences the activity of these anti-recombinases

384   directly or controls their access to the damaged replication fork and/or the Rad51 filament itself.

385   Given that BOD1L and BLM co-associate, it is tempting to speculate that BOD1L regulates BLM

386   activity directly. Alternatively, since the Rad51 paralogues stabilise Rad51 nucleofilaments by

387   blocking the translocase activities of anti-recombinogenic helicases (Amunugama *et al.*, 2013; Liu

388   *et al.,* 2011), BOD1L may act in an analogous fashion to regulate access of BLM/Fbh1 to Rad51,

389   ultimately stabilising Rad51 nucleofilaments at damaged replication forks. As a consequence,

390   ablating BOD1L could promote uncontrolled BLM-DNA2-dependent resection, and allow

391   BLM/Fbh1-dependent dissolution of Rad51 filaments.

392

393   **BOD1L functions in the latter stages of the FA/HR pathway**

394   The phenotypic similarities between BOD1L-deficient cells and FA-defective cells,

395   particularly after ICL induction, suggest that BOD1L functions as part of the FA/HR pathway.

396   Indeed, loss of BOD1L and core/downstream FA components (namely FANCA and BRCA2) are

397   epistatic for MMC hypersensitivity and fork protection. In further support, the increased fork

398   resection apparent in both BOD1L-deficient and FANCD2-null cells is attributable to the nucleolytic

399   activity of DNA2 (Karanja *et al.*, 2014). However, since BOD1L is not required for mono-

400   ubiquitylation or relocalisation of FANCD2 to sites of DNA damage, and also that the chromatin

401   localisation/retention of Rad51 is unaffected in cells lacking FA core components or FANCD2/I

402   (Ohashi *et al.,* 2005; Godthelp et al., 2006), this indicates that BOD1L functions in the latter stages

403 of the FA pathway, downstream of FANCD2/I. This also suggests that fork protection mechanisms

404 independent of Rad51-loading (but perhaps dependent on Rad51 activity) also exist.

405

406 **Increased origin firing contributes to genome instability in BOD1L deficient cells**

407   We have shown that cells depleted of BOD1L exhibit increased new origin firing following

408 the induction of replication stress. We hypothesise that this elevated origin firing is a cellular

409 response to an inability to complete DNA replication, caused by the uncontrolled resection of

410 stalled forks due to a failure to stabilise Rad51. This results in elevated levels of mitotic replication,

411 UFBs, G1 53BP1 bodies and severe chromosomal instability.

412   Whether Rad51 defects alone promote new origin firing is currently unclear. Increased new

413 origin firing does not occur in human cells depleted of Rad51 or in BRCA2-null CHO cells following

414 HU (Petermann *et al.,* 2010; Jones *et al.*, 2014), but increased new origin firing has been shown in

415 BLM-deficient cells and those lacking PALB2 (Davies *et al.*, 2007; Nikkila *et al.*, 2013). It therefore

416 remains to be determined whether the inability of BOD1L-depleted cells to retain Rad51 at stalled

417 replication forks contributes to the increase in origin firing. In spite of this, we predict that the

418 increased origin firing in BOD1L deficient cells could contribute to genome instability, perhaps due

419 to collisions between newly fired origins and damaged forks lying in close proximity.

420

421 **Summary**

422   Taken together, our data leads us to propose the following model (**Figure 7F**): BOD1L

423 forms an essential component of the fork protection machinery. Upon stalling of a replication fork

424 (for example by an ICL), limited nucleolytic resection allows Rad51-dependent HR and

425 repair/restart of the stalled fork. BOD1L acts to stabilise Rad51 at such structures by protecting

426 Rad51 nucleofilaments from the activities of Fbh1/BLM. In the absence of BOD1L, Rad51 is

427 displaced from ssDNA by Fbh1/BLM, rendering the fork susceptible to uncontrolled resection by

428 DNA2, and leading to catastrophic genome instability, in part mediated by the presence of under-

429 replicated DNA.

430

17

EXPERIMENTAL PROCEDURES

Cell culture and generation of cell lines

A549, HeLa, HeLa S3, H1299 and HeLa-FUCCI cells were grown in Dulbecco's modified Eagle's medium supplemented with 10% fetal bovine serum (FBS) (Gibco) and penicillin/streptomycin. HeLa-CFlap-BOD1L and U-2-OS SUPER-RPA cells were cultivated as above in the presence of 200 µg/ml Geneticin. U-2-OS and U-2-OS-PALB2-GFP cells were cultured in McCoys 5A medium, supplemented with 10% FBS and penicillin/streptomycin. DT40 cells were cultured in RPMI 1640 medium (Invitrogen) supplemented with 7% FBS, 3% chicken serum, and 10 µM β-mercaptoethanol. Further details of DT40s, HeLa-CFlap-mBOD1L cells, siRNA transfections and clonogenic survival assays are given in the Extended Experimental Procedures.

iPOND

iPOND was performed on HeLa S3 as described previously (Sirbu *et al.,* 2013) with some modifications to allow for improved detection of high molecular weight proteins, which are described in Extended Experimental Procedures. In brief, newly synthesized DNA was labelled with 10µM EdU, cells were fixed in 1% formaldehyde, permeablised and the Click reaction was performed using Azide-PEG (3+3)-S-S-Biotin Conjugate (Click ChemistryTools). Following sonication, EdU labelled DNA was precipitated using Streptavidin beads and eluted in buffer containing DDT.

Statistical analyses

Differences in survival assays were analysed by two-way ANOVA. Statistical differences in all cases were determined by Student's t-test, except for fork asymmetry, which was analysed by Mann-Whitney rank sum test. In all cases: NS = $p>0.05$; * = $p<0.05$; ** = $p<0.01$; *** = $p<0.001$.

AUTHOR CONTRIBUTIONS

MRH, JJR and GSS designed the study, performed experiments and wrote the manuscript. AW performed iPOND. VB made HeLa-CFlap-mBOD1L cells and performed CFlap IPs. ANB and JN created BOD1L-null DT40s. ESM and AZ performed experiments and created reagents. ELR assisted with DNA combing. ND performed FISH. TS, SJB and WN supervised and advised on experiments. All authors contributed to manuscript revisions.

REFERENCES

Adamo, A., Collis, S.J., Adelman, C.A., Silva, N., Horejsi, Z., Ward, J.D., Martinez-Perez, E., Boulton, S.J., and La Volpe, A. (2010). Preventing nonhomologous end joining suppresses DNA repair defects of Fanconi anemia. Molecular cell 39, 25-35.

Akkari, Y.M., Bateman, R.L., Reifsteck, C.A., D'Andrea, A.D., Olson, S.B., and Grompe, M. (2001). The 4N cell cycle delay in Fanconi anemia reflects growth arrest in late S phase. Molecular genetics and metabolism 74, 403-412.

Amunugama, R., Groden, J., and Fishel, R. (2013). The HsRAD51B-HsRAD51C stabilizes the HsRAD51 nucleoprotein filament. DNA repair 12, 723-732.

Barlow, J.H., Faryabi, R.B., Callen, E., Wong, N., Malhowski, A., Chen, H.T., Gutierrez-Cruz, G., Sun, H.W., McKinnon, P., Wright, G., et al. (2013). Identification of early replicating fragile sites that contribute to genome instability. Cell 152, 620-632.

Bhattacharyya, A., Ear, U.S., Koller, B.H., Weichselbaum, R.R., and Bishop, D.K. (2000). The breast cancer susceptibility gene BRCA1 is required for subnuclear assembly of Rad51 and survival following treatment with the DNA cross-linking agent cisplatin. The Journal of biological chemistry 275, 23899-23903.

Bugreev, D.V., Yu, X., Egelman, E.H., and Mazin, A.V. (2007). Novel pro- and anti-recombination activities of the Bloom's syndrome helicase. Genes & development 21, 3085-3094.

Chan, K.L., North, P.S., and Hickson, I.D. (2007). BLM is required for faithful chromosome segregation and its localization defines a class of ultrafine anaphase bridges. The EMBO journal 26, 3397-3409.

502 Chan, K.L., Palmai-Pallag, T., Ying, S., and Hickson, I.D. (2009). Replication stress induces sister-

503 chromatid bridging at fragile site loci in mitosis. Nature cell biology 11, 753-760.

504

505 Chen, H., Lisby, M., and Symington, L.S. (2013). RPA coordinates DNA end resection and

506 prevents formation of DNA hairpins. Molecular cell 50, 589-600.

507

508 Conti, C., Seiler, J.A., and Pommier, Y. (2007). The mammalian DNA replication elongation

509 checkpoint: implication of Chk1 and relationship with origin firing as determined by single DNA

510 molecule and single cell analyses. Cell Cycle 6, 2760-2767.

511

512 Costanzo, V. (2011). Brca2, Rad51 and Mre11: performing balancing acts on replication forks.

513 DNA repair 10, 1060-1065.

514

515 Davies, S.L., North, P.S., and Hickson, I.D. (2007). Role for BLM in replication-fork restart and

516 suppression of origin firing after replicative stress. Nature structural & molecular biology 14, 677-

517 679.

518

519 Durkin, S.G., and Glover, T.W. (2007). Chromosome fragile sites. Annual review of genetics 41,

520 169-192.

521

522 Esashi, F., Galkin, V.E., Yu, X., Egelman, E.H., and West, S.C. (2007). Stabilization of RAD51

523 nucleoprotein filaments by the C-terminal region of BRCA2. Nature Structural & Molecular Biology

524 14, 468-474.

525

526 Fugger, K., Mistrik, M., Danielsen, J.R., Dinant, C., Falck, J., Bartek, J., Lukas, J., and Mailand, N.

527 (2009). Human Fbh1 helicase contributes to genome maintenance via pro- and anti-recombinase

528 activities. The Journal of cell biology 186, 655-663.

529

530 Garaycoechea, J.I., and Patel, K.J. (2014). Why does the bone marrow fail in Fanconi anemia?

531 Blood 123, 26-34.

532

533 Gari, K., and Constantinou, A. (2009). The role of the Fanconi anemia network in the response to

534 DNA replication stress. Critical reviews in biochemistry and molecular biology 44, 292-325.

535

536 Godthelp, B.C., Wiegant, W.W., Waisfisz, Q., Medhurst, A.L., Arwert, F., Joenje, H., and

537 Zdzienicka, M.Z. (2006). Inducibility of nuclear Rad51 foci after DNA damage distinguishes all

538 Fanconi anemia complementation groups from D1/BRCA2. Mutation research 594, 39-48.

539

540 Heinrich, M.C., Hoatlin, M.E., Zigler, A.J., Silvey, K.V., Bakke, A.C., Keeble, W.W., Zhi, Y.,

541 Reifsteck, C.A., Grompe, M., Brown, M.G., et al. (1998). DNA cross-linker-induced G2/M arrest in

542 group C Fanconi anemia lymphoblasts reflects normal checkpoint function. Blood 91, 275-287.

543

544 Howlett, N.G., Taniguchi, T., Durkin, S.G., D'Andrea, A.D., and Glover, T.W. (2005). The Fanconi

545 anemia pathway is required for the DNA replication stress response and for the regulation of

546 common fragile site stability. Human molecular genetics 14, 693-701.

547

548 Jones, R.M., Kotsantis, P., Stewart, G.S., Groth, P., and Petermann, E. (2014). BRCA2 and

549 RAD51 promote double-strand break formation and cell death in response to gemcitabine.

550 Molecular cancer therapeutics 13, 2412-2421.

551

552 Karanja, K.K., Lee, E.H., Hendrickson, E.A., and Campbell, J.L. (2014). Preventing over-resection

553 by DNA2 helicase/nuclease suppresses repair defects in Fanconi anemia cells. Cell Cycle 13,

554 1540-1550.

555

556 Kim, T.M., Son, M.Y., Dodds, S., Hu, L., Luo, G., and Hasty, P. (2015). RECQL5 and BLM exhibit

557 divergent functions in cells defective for the Fanconi anemia pathway. Nucleic Acids Research 43,

558 893-903.

559

560 Kohzaki, M., Hatanaka, A., Sonoda, E., Yamazoe, M., Kikuchi, K., Vu Trung, N., Szuts, D., Sale,

561 J.E., Shinagawa, H., Watanabe, M., et al. (2007). Cooperative roles of vertebrate Fbh1 and Blm

562 DNA helicases in avoidance of crossovers during recombination initiated by replication fork

563 collapse. Molecular and cellular biology 27, 2812-2820.

564

565 Koundrioukoff, S., Carignon, S., Techer, H., Letessier, A., Brison, O., and Debatisse, M. (2013).

566 Stepwise activation of the ATR signaling pathway upon increasing replication stress impacts fragile

567 site integrity. PLoS genetics 9, e1003643.

568

569

570 Liu, J., Renault, L., Veaute, X., Fabre, F., Stahlberg, H., and Heyer, W.D. (2011). Rad51

571 paralogues Rad55-Rad57 balance the antirecombinase Srs2 in Rad51 filament formation. Nature

572 479, 245-248.

573

574 Lukas, C., Savic, V., Bekker-Jensen, S., Doil, C., Neumann, B., Pedersen, R.S., Grofte, M., Chan,

575 K.L., Hickson, I.D., Bartek, J., et al. (2011). 53BP1 nuclear bodies form around DNA lesions

576 generated by mitotic transmission of chromosomes under replication stress. Nature cell biology 13,

577 243-253.

578

579 Matsuoka, S., Ballif, B.A., Smogorzewska, A., McDonald, E.R., 3rd, Hurov, K.E., Luo, J.,

580 Bakalarski, C.E., Zhao, Z., Solimini, N., Lerenthal, Y., et al. (2007). ATM and ATR substrate

581 analysis reveals extensive protein networks responsive to DNA damage. Science 316, 1160-1166.

582

583 Naim, V., and Rosselli, F. (2009a). The FANC pathway and BLM collaborate during mitosis to

584 prevent micro-nucleation and chromosome abnormalities. Nature cell biology 11, 761-768.

585

586 Naim, V., and Rosselli, F. (2009b). The FANC pathway and mitosis: a replication legacy. Cell

587 Cycle 8, 2907-2911.

588

589 Nikkila, J., Parplys, A.C., Pylkas, K., Bose, M., Huo, Y., Borgmann, K., Rapakko, K., Nieminen, P.,

590 Xia, B., Pospiech, H., et al. (2013). Heterozygous mutations in PALB2 cause DNA replication and

591 damage response defects. Nature communications 4, 2578.

592

593 Ohashi, A., Zdzienicka, M.Z., Chen, J., and Couch, F.J. (2005). Fanconi anemia complementation

594 group D2 (FANCD2) functions independently of BRCA2- and RAD51-associated homologous

595 recombination in response to DNA damage. The Journal of biological chemistry 280, 14877-14883.

596

597 Petermann, E., Orta, M.L., Issaeva, N., Schultz, N., and Helleday, T. (2010). Hydroxyurea-stalled

598 replication forks become progressively inactivated and require two different RAD51-mediated

599 pathways for restart and repair. Molecular cell 37, 492-502.

600

601 Porter, I.M., McClelland, S.E., Khoudoli, G.A., Hunter, C.J., Andersen, J.S., McAinsh, A.D., Blow,

602 J.J., and Swedlow, J.R. (2007). Bod1, a novel kinetochore protein required for chromosome

603 biorientation. The Journal of cell biology 179, 187-197.

604

605 Porter, I.M., Schleicher, K., Porter, M., and Swedlow, J.R. (2013). Bod1 regulates protein

606 phosphatase 2A at mitotic kinetochores. Nature communications 4, 2677.

607

608 Rodriguez-Lopez, A.M., Jackson, D.A., Iborra, F., and Cox, L.S. (2002). Asymmetry of DNA

609 replication fork progression in Werner's syndrome. Aging cell 1, 30-39.

610

611 Schlacher, K., Christ, N., Siaud, N., Egashira, A., Wu, H., and Jasin, M. (2011). Double-strand

612 break repair-independent role for BRCA2 in blocking stalled replication fork degradation by

613 MRE11. Cell 145, 529-542.

614

615 Schlacher, K., Wu, H., and Jasin, M. (2012). A distinct replication fork protection pathway connects

616 Fanconi anemia tumor suppressors to RAD51-BRCA1/2. Cancer cell 22, 106-116.

617

618   Schoder, C., Liehr, T., Velleuer, E., Wilhelm, K., Blaurock, N., Weise, A., and Mrasek, K. (2010).

619   New aspects on chromosomal instability: chromosomal break-points in Fanconi anemia patients

620   co-localize on the molecular level with fragile sites. International journal of oncology 36, 307-312.

621

622   Sirbu, B.M., McDonald, W.H., Dungrawala, H., Badu-Nkansah, A., Kavanaugh, G.M., Chen, Y.,

623   Tabb, D.L., and Cortez, D. (2013). Identification of proteins at active, stalled, and collapsed

624   replication forks using isolation of proteins on nascent DNA (iPOND) coupled with mass

625   spectrometry. The Journal of biological chemistry 288, 31458-31467.

626

627   Smogorzewska, A., Matsuoka, S., Vinciguerra, P., McDonald, E.R., 3rd, Hurov, K.E., Luo, J., Ballif,

628   B.A., Gygi, S.P., Hofmann, K., D'Andrea, A.D., et al. (2007). Identification of the FANCI protein, a

629   monoubiquitinated FANCD2 paralog required for DNA repair. Cell 129, 289-301.

630

631   Sturzenegger, A., Burdova, K., Kanagaraj, R., Levikova, M., Pinto, C., Cejka, P., and Janscak, P.

632   (2014). DNA2 cooperates with the WRN and BLM RecQ helicases to mediate long-range DNA end

633   resection in human cells. The Journal of biological chemistry 289, 27314-27326.

634

635   Toledo, L.I., Altmeyer, M., Rask, M.B., Lukas, C., Larsen, D.H., Povlsen, L.K., Bekker-Jensen, S.,

636   Mailand, N., Bartek, J., and Lukas, J. (2013). ATR prohibits replication catastrophe by preventing

637   global exhaustion of RPA. Cell 155, 1088-1103.

638

639

640   Walden, H., and Deans, A.J. (2014). The Fanconi anemia DNA repair pathway: structural and

641   functional insights into a complex disorder. Annual review of biophysics 43, 257-278.

642

643   Xia, B., Dorsman, J.C., Ameziane, N., de Vries, Y., Rooimans, M.A., Sheng, Q., Pals, G., Errami,

644   A., Gluckman, E., Llera, J., et al. (2007). Fanconi anemia is associated with a defect in the BRCA2

645   partner PALB2. Nature genetics 39, 159-161.

646

647 Xia, B., Sheng, Q., Nakanishi, K., Ohashi, A., Wu, J., Christ, N., Liu, X., Jasin, M., Couch, F.J., and

648 Livingston, D.M. (2006). Control of BRCA2 cellular and clinical functions by a nuclear partner,

649 PALB2. Molecular cell 22, 719-729.

650

651 Xue, X., Raynard, S., Busygina, V., Singh, A.K., and Sung, P. (2013). Role of replication protein A

652 in double holliday junction dissolution mediated by the BLM-Topo IIIalpha-RMI1-RMI2 protein

653 complex. The Journal of biological chemistry 288, 14221-14227.

654

655 Ying, S., Hamdy, F.C., and Helleday, T. (2012). Mre11-dependent degradation of stalled DNA

656 replication forks is prevented by BRCA2 and PARP1. Cancer Research 72, 2814-2821.

657

658 Yuan, S.S., Lee, S.Y., Chen, G., Song, M., Tomlinson, G.E., and Lee, E.Y. (1999). BRCA2 is

659 required for ionizing radiation-induced assembly of Rad51 complex in vivo. Cancer research 59,

660 3547-3551.

661

662 Zeman, M.K., and Cimprich, K.A. (2014). Causes and consequences of replication stress. Nature

663 cell biology 16, 2-9.

664

665 Zhang, F., Fan, Q., Ren, K., and Andreassen, P.R. (2009). PALB2 functionally connects the breast

666 cancer susceptibility proteins BRCA1 and BRCA2. Molecular cancer research : MCR 7, 1110-

667 1118.

668

FIGURE LEGENDS

670 **Figure 1: BOD1L is present at newly-replicated DNA, and ensures cellular viability after**

671 **replication stress. (A)** *Upper:* Schematic of human BOD1L and BOD1 domain structure and

672 ATM/ATR phosphorylation sites. *Lower:* Amino acid sequence alignment of BOD1L and BOD1.

673 Conserved residues (red) and similar residues (+) are denoted. **(B)** Immunoblotting of EdU-

674 coprecipitates from HeLa S3 cells. **(C-D)** HeLa cells were transfected with the indicated siRNAs,

675 and pulsed with 10 µM EdU for 10 minutes before pre-extraction/fixation. EdU incorporation was

676 visualised with Click-iT chemistry, and detection of protein-protein associations were performed

677 using a fluorescently labelled PLA probe along with the indicated antibodies. (C) shows

678 quantification of PLA signals/nucleus from at least 100 cells (n = 3; lines denote mean values), and

679 representative images are shown (D). Scale bars = 10 µm. **(E)** HeLa nuclear cell extracts were

680 subjected to IP with the indicated antibodies, and inputs and immunoprecipitates were analyzed by

681 immunoblotting. Blots originate from a single gel. A white line denotes removal of irrelevant lanes.

682 **(F)** The survival of HeLa cells transfected with the indicated siRNA following exposure to

683 mitomycin C (MMC) or hydroxyurea (HU) was assessed by colony survival assay. **(G)** Micronuclei

684 formation following DNA damage was assessed in siRNA-transfected HeLa cells by fluorescence

685 microscopy. Plots (F)-(G) represent mean data from four independent experiments; error bars =

686 SEM. See also Figure S1.

687

688 **Figure 2: BOD1L is functionally distinct from BOD1. (A)**. Whole cell extracts (WCE) of HeLa

689 cells transfected with the indicated siRNA were analysed by immunoblotting after exposure to 50

690 ng/ml MMC for the denoted times. **(B)** HeLa cells from (A) were exposed to 50 ng/ml MMC for 24

691 h, and micronuclei enumerated. **(C-D)** The survival of HeLa cells transfected with the indicated

692 siRNA was assessed by colony survival assay as in **Figure 1F**. **(E-F)** Untreated HeLa cells from

693 (A) were immunostained with antibodies to α-tubulin and PCNT1, and the percentage of mitotic

694 cells in each stage of mitosis (E), or their ability to form centrosomes (F), was analysed by

695 immunofluorescence. Scale bars = 10 µm. Data represent mean ± SEM of three independent

696 experiments.

697

Figure 3: BOD1L knockdown leads to problematic resolution of replication stress. (A) The

percentage of micronuclei positive for either 53BP1 or CENPA was quantified by

immunofluorescence microscopy in HeLa cells transfected with indicated siRNAs after exposure to

50 ng/ml MMC for 24 h. **(B)** The percentage of mitotic cells with PICH-positive UFBs was

quantified in transfected HeLa cells after exposure to 250 ng/ml MMC for 3 h and release into fresh

media for 36 h. **(C)** The mean percentage of PICH-positive UFBs with terminal FANCD2 foci in

mitotic cells from (B) is indicated. **(D)** Cells from (B) were pulsed with 10 μM EdU for 45 minutes

before fixation. Mitotic EdU incorporation was visualised with Click chemistry labelling, and the

mean number of EdU foci per mitotic cell, and merged representative images, are shown. Scale

bars = 10 μm. **(E-F)** HeLa-FUCCI cells were siRNA-transfected, and exposed to 50 ng/ml MMC for

24 h. (E) WCE were analysed by immunoblotting. Loading control denotes a non-specific protein

detected by anti-BOD1L antibody. (F) The number of 53BP1 bodies in RFP-positive (i.e. G1) cells

was enumerated. **(G)** Damage to metaphase chromosomes from HeLa cells subjected to the

indicated siRNAs was determined by Geimsa staining and light microscopy. *Upper:* Graphs

integrate data from three independent experiments (n = 150; lines denote mean values). *Lower:*

Representative metaphase spreads are shown, with chromosomal damage denoted by

arrowheads. **(H)** Cells from (G) were analysed by FISH using probes against FRA16D. Plots

represent mean ± SEM of three independent experiments. See also Figure S2.

Figure 4: BOD1L knockdown increases origin firing after replication stress and destabilises

replication forks. (A-B) The cell cycle profiles of HeLa cells subjected to the indicated siRNAs

were analysed by flow cytometry. Representative profiles from untreated cells (A) or after exposure

to 250 ng/ml MMC for 3 h (B) are shown. **(C-D)** DNA fibre analysis of HeLa cells transfected with

the indicated siRNAs. Cells were pulsed with CldU, exposed to 2 mM HU for 2 h, and pulsed with

IdU. Plots indicate ratios of left/right fork lengths of bidirectional replication forks travelling from a

single origin. Lines denote median ratios (C). DNA fibres were enumerated, and the percentage of

new origins (IdU-labelled only) is displayed (D). **(E)** Transfected cells from (C) were exposed to 50

ng/ml MMC for 24 h, and pulsed sequentially with CldU and IdU. DNA fibres were quantified, and

the percentage of new origins is displayed. **(F)** WCE of HeLa cells transfected as above and

exposed to MMC for the indicated times were analysed by immunoblotting. *Chronic = 50 ng/ml MMC. **Acute = 250 ng/ml MMC for 3h followed by wash out. Times for acute exposure indicate h post washout. Plots represent mean ± SEM of at least three independent experiments. See also Figure S3.

Figure 5: BOD1L prevents excessive ssDNA formation and RPA2 hyper-phosphorylation after MMC exposure. (A) Soluble and chromatin fractions of U-2-OS cells transfected with the indicated siRNAs, and exposed to 100 ng/ml MMC for 24 h, were analysed by immunoblotting. Loading control denotes a non-specific protein detected by anti-BOD1L antibody. Blots originate from a single gel. A white line denotes removal of superfluous lanes. **(B)** RPA foci formation was analysed in HeLa cells transfected as above and exposed to 50 ng/ml MMC for the denoted times. **(C)** Native BrdU foci formation in U-2-OS cells by fluorescence microscopy. Cells were transfected with the indicated siRNAs, and BrdU added for 24 h. Cells were exposed to 50 ng/ml MMC for a further 24 h in the presence of BrdU, and immunostained with antibodies to BrdU and γH2AX. Foci formation was analysed (see **Figure S4B**), and enumerated. **(D)** WCE of HeLa cells transfected as in (B), and exposed to MMC for the indicated times, were analysed by immunoblotting. *Chronic = 50 ng/ml MMC. **Acute = 250 ng/ml MMC for 3h followed by wash out. Times for acute exposure indicate h post washout. **(E)** Phospho-RPA (S4/S8) and RPA foci formation in transfected HeLa cells exposed to 50 ng/ml MMC for 24 h. **(F)** The number of double positive cells from (E) was enumerated. **(G)** Detection of protein-protein interactions was performed using a fluorescently labelled PLA probe in HeLa cells from (B). The plot shows quantification of PLA signals/nucleus from at least 100 cells (n=3; lines denote mean values), and representative images are shown. Plots represent mean ± SEM of three independent experiments. Scale bars = 10 µm. See also Figure S4.

Figure 6: BOD1L is required to suppress aberrant fork resection after replication stress, and is required for efficient Rad51 chromatin loading. (A) Fork degradation was analysed in U-2-OS cells. Cells were transfected with the indicated siRNAs, pulsed for 20 min each with CldU and
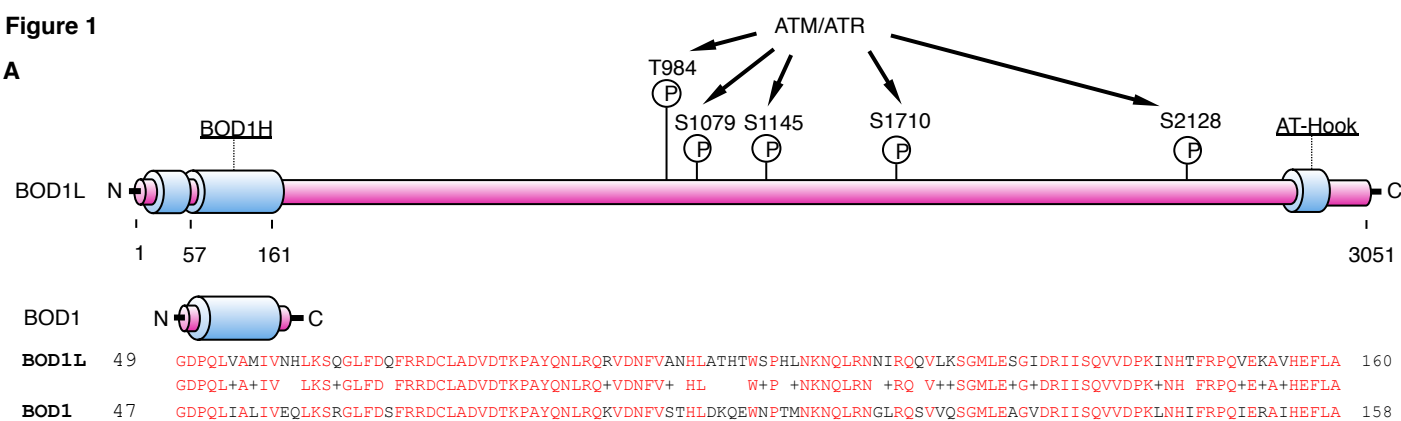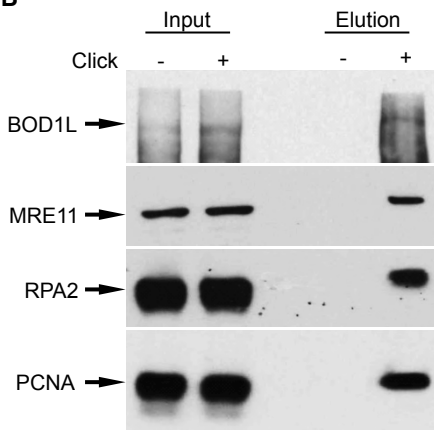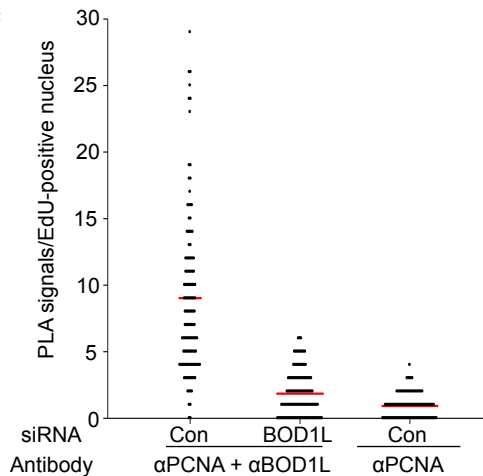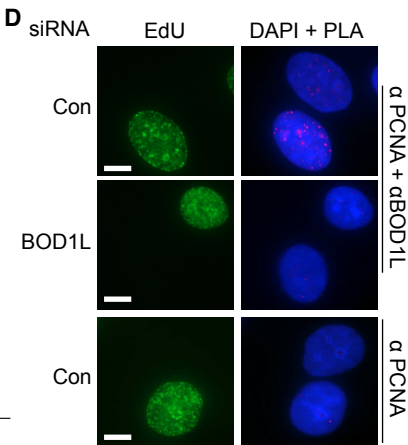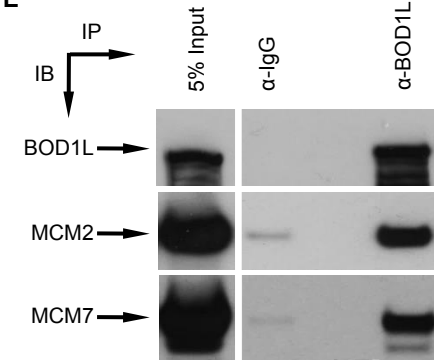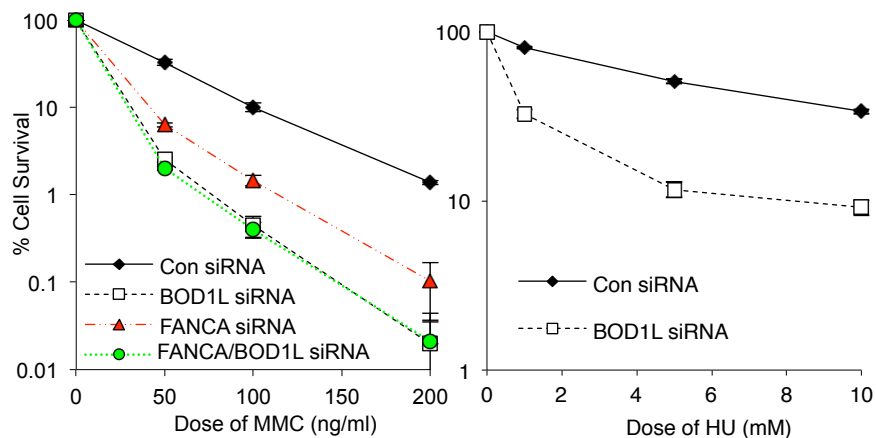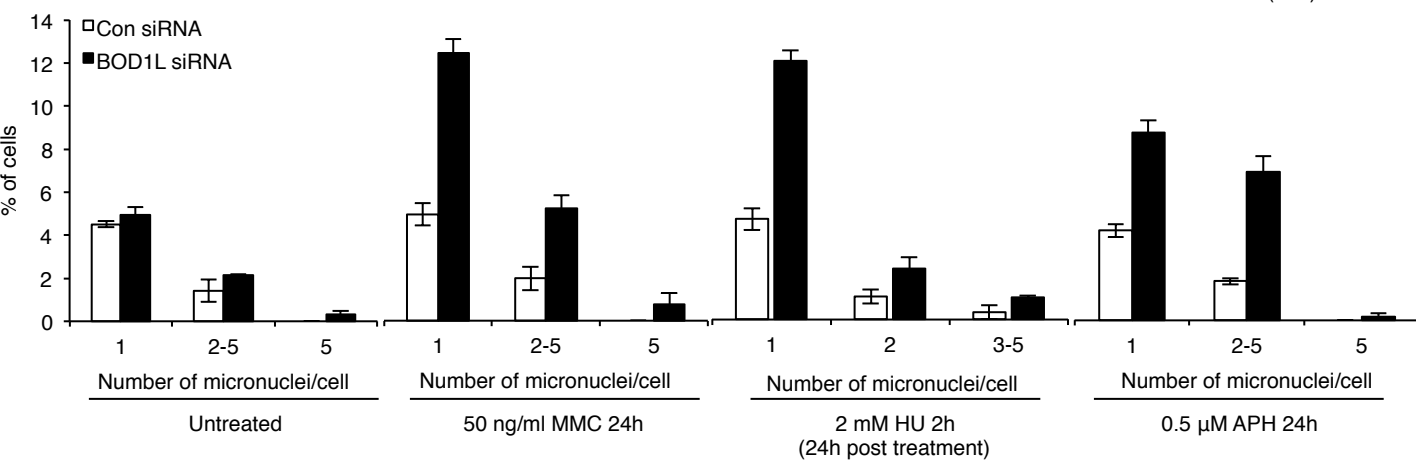
IdU, and exposed to 4 mM HU for 5 h. DNA was visualised with antibodies to CldU and IdU, and

plots denote the average ratios of IdU:CldU label lengths from three independent experiments.

Arrows indicate mean values (see **Figure S5B**). **(B)** HeLa nuclear cell extracts were subjected to

IP with the denoted antibodies, and inputs and immunoprecipitates were analyzed by

immunoblotting. Blots originate from a single gel. A white line denotes removal of irrelevant lanes.

(C) Fork degradation in U-2-OS cells transfected and treated as in (A) was analysed. Where

appropriate cells were treated with Mirin for the duration of the HU pulse (see **Figure S5H**). **(D)**

Micronuclei formation was quantified in HeLa cells transfected with the indicated siRNAs and

treated with 50 ng/ml MMC for 24 h. **(E)** Damage to metaphase chromosomes from cells (D) was

analysed (n = 150; lines denote mean values). **(F)** Rad51 foci formation was analysed in siRNA-

transfected HeLa cells, and exposed to 50 ng/ml MMC for the indicated times. Scale bars = 10 µm.

(G) Soluble and chromatin fractions from **Figure 5A** were analysed by immunoblotting. **(H)** Foci

formation of BRCA1 and BRCA2 was analysed in HeLa cells from (F). Alternatively, U-2-OS-

PALB2-GFP cells were transfected with the indicated siRNAs, exposed to 50 ng/ml MMC for 24 h,

and fixed. In both cases mean percentage of cells with foci are shown (see **Figures S6G-I**). Plots

(D-H) represent mean ± SEM of three independent experiments. See also Figures S5 and S6.

Figure 7: BOD1L stabilises Rad51 chromatin loading to prevent excessive replication fork

resection. (A-B) RPA2/phospho-RPA2 S4/S8 (A) or Rad51 (B) foci formation was analysed in

HeLa cells transfected with the indicated siRNAs and exposed to 50 ng/ml MMC for 24 h. Scale

bars = 10 µm. **(C)** Fork degradation was assessed in U-2-OS cells transfected with the indicated

siRNAs as described in **Figure 6A** (see also **Figure S7F**). **(D)** Damage to metaphase

chromosomes in HeLa cells from (A) was analysed (n = 100; lines denote mean values). **(E)** HeLa

nuclear cell extracts subjected to IP with the indicated antibodies, and inputs and

immunoprecipitates were analyzed by immunoblotting. Blots originate from a single gel. A white

line denotes removal of irrelevant lanes. Plots (C-D) represent mean ± SEM of three independent

experiments. **(F)** Model of BOD1L function to promote Rad51 nucleofilament stability and prevent

uncontrolled resection of replication forks. Upon replication fork stalling, forks undergo minimal

nucleolytic processing (i), allowing Rad51 loading/protection by BRCA1/BRCA2/PALB2 (ii). BOD1L

30

784   acts to stabilise Rad51 nucleofilaments by protecting them from the activities of BLM/Fbh1 (iii),

785   thus preventing uncontrolled resection and allowing Rad51-mediated repair/restart of forks,

786   ultimately maintaining genome stability. In the absence of BOD1L, BLM/Fbh1 act to remove Rad51

787   from such forks exposing them to uncontrolled DNA2-dependent processing (iv). To compensate

788   for this fork instability, increased new origin firing occurs. When combined with uncontrolled

789   resection of replication forks, this leads to catastrophic genome instability (v). See also Figure S7.

Figure 1

A

BOD1H

ATM/ATR

T984

S1079 S1145 S1710 S2128

AT-Hook

BOD1L   N   C

1   57   161   3051

BOD1   N   C

BOD1L 49 GDPQLVAMIVNHLKSQGLFDQFRRDCLADVDTKPAYQNLRQRVDNFVANHLATHTWSPHLNKNQLRNNIRQQVLKSGMLESGIDRIISQVVDPKINHTFRPQVEKAVHEFLA 160
           GDPQL+A+IV LKS+GLFD FRRDCLADVDTKPAYQNLRQ+VDNFV+ HL W+P +NKNQLRN +RQ V++SGMLE+G+DRIISQVVDPK+NH FRPQ+E+A+HEFLA
BOD1   47 GDPQLIALIVEQLKSRGLFDSFRRDCLADVDTKPAYQNLRQKVDNFVSTHLDKQEWNPTMNKNQLRNGLRQSVVQSGMLEAGVDRIISQVVDPKLNHIFRPQIERAIHEFLA 158

B

C

D

E

F

G

Figure 2

Figure 3

Figure 4

A

Con siRNA	G1:57.7% S:16.4% G2/M:23.9%

BOD1L siRNA	G1:54.5% S:18.6% G2/M:25.1%

B

Time (h) post MMC	0	24	48

C

Left fork length/right fork length (ratio)

***

Con siRNA + HU   BOD1L siRNA + HU

D

% of all CldU labelled

☐ Con siRNA   ■ BOD1L siRNA

Unt   + HU

2nd label origin

E

% of all CldU labelled

☐ Con siRNA   ■ BOD1L siRNA

Unt   + MMC

2nd label origin

F

	Control siRNA					BOD1L siRNA				
		Chronic*		Acute**			Chronic*		Acute**	
Time (h) after MMC	0	24	48	24	48	0	24	48	24	48

CHK1 S345-P →

CHK1 S317-P →

CHK1 →

Figure 5

Figure 6

Figure 7

Figure S1

A

Protein ID	No. of peptides
PCNA	**9**
Pol δ p66 subunit	3
Pol δ p50 subunit	7
Pol δ cat. subunit	20
Pol α B subunit	3
Pol α cat. subunit	9
RFC1	5
RFC2	5
RFC3	6
RFC4	10
RFC5	7
MCM2	21
MCM3	22
MCM4	26
MCM5	17
MCM6	17
MCM7	23
RPA1	**16**
RPA2	3
RPA3	**1**
PSF3	1
BOD1L	6

B

IP
IB

Input   αGFP

Parental   CFlap-mBod1L   Parental   CFlap-mBod1L

CFlap-mBOD1L (αGFP) →

MCM2 →

C

% Cell Survival

UV (J/m2)

Con siRNA
BOD1L siRNA

Dose of APH (nM)

Con siRNA   BOD1L siRNA
BOD1L
H2A

D

% of Cells

Control siRNA
BOD1L siRNA

Number of micronuclei/cell
1   2-5   <5   Bridging

U-2-OS

1   2-5   <5   Bridging

H1299

E

WT cl. 18   BOD1L cl. 1   BOD1L cl. 2

ScrF1 + ScrR1

ScrF2 + ScrR2

ScrF3 + ScrR3

ScrF4 + ScrR4

Control

F

Gg*BOD1L* locus

1 2 3 4 5 6 7 8 9 10

BOD1L targeting vectors

5' arm   puroR   3' arm   5' arm   hygroR   3' arm

Targeted locus

ScrF1   ScrF2   ScrF3   ScrF4
puroR   5 6 7 8 9 10   hygroR   10
ScrR1   ScrR2   ScrR3   ScrR4
2.6kb   2.7kb   3.5kb   4.1kb

G

% Cell Survival

MMC (ng/ml)

WT cl.18
BOD1L cl. 1
BOD1L cl. 2

***

H

% of Cells

WT cl. 18
BOD1L cl. 1
BOD1L cl. 2

Number of micronuclei/cell
1   2-5   5+   1   2-5   5+

Untreated   + MMC

*   *   *   *

Figure S2

Figure S3

Figure S4

Figure S5

A

(Histogram of % of forks vs IdU:CldU ratio)

Markers: 0.66 (orange), 0.67 (green), 0.69 (red), 0.97 (black)

Legend:
- Con siRNA +HU (black)
- BRCA1 siRNA + HU (green)
- BOD1L siRNA + HU (red)
- BOD1L/BRCA1 siRNA + HU (orange)

Western blot:
- siRNA: Con, BRCA1, BRCA1 + BOD1L
- BOD1L
- BRCA1
- Loading Control

B

	Average IdU:CldU ratio	SEM
Con siRNA	1.02	0.01
BRCA1 siRNA	1.02	0.01
BRCA2 siRNA	1.02	0.03
BOD1L siRNA	1.00	0.02
BOD1L/BRCA1 siRNA	0.99	0.03
BOD1L/BRCA2 siRNA	1.01	0.01
Con siRNA + HU	0.97	0.03
BRCA1 siRNA + HU	0.67	0.04
BRCA2 siRNA + HU	0.69	0.02
BOD1L siRNA + HU	0.68	0.03
BOD1L/BRCA1 siRNA + HU	0.66	0.03
BOD1L/BRCA2 siRNA + HU	0.64	0.02

C

(% Cell Survival vs Dose of MMC (ng/ml))

Legend:
- Con siRNA
- BOD1L siRNA
- BRCA2 siRNA
- BRCA2/BOD1L siRNA

D

Western blot:
- siRNA: Con, BOD1L, BRCA2, BRCA2 + BOD1L
- BOD1L
- BRCA2
- Loading Control

E

(% of RPA/phospho-RPA S4/S8 positive cells vs Untreated / MMC)

Legend:
- Con siRNA
- BOD1L siRNA
- BRCA2 siRNA
- BOD1L/BRCA2 siRNA

F

(% of RPA/phospho-RPA S4/S8 positive cells)

X-axis: + MMC, EXO1 siRNA + MMC, DNA2 siRNA + MMC

Legend:
- Con siRNA
- BOD1L siRNA

G

Western blot:
siRNA: Con, BOD1L, DNA2, BOD1L/DNA2, EXO1, BOD1L/EXO1

+ MMC 24 h

- BOD1L
- DNA2
- EXO1
- RPA2-P S4/S8
- RPA2
- γH2AX
- H2A

H

	Untreated		+ HU	
	Average IdU:CldU ratio	SEM	Average IdU:CldU ratio	SEM
Con siRNA	1.01	0.03	1.03	0.01
BOD1L siRNA	1.02	0.01	0.70	0.02
BOD1L/DNA2 siRNA	1.02	0.04	0.99	0.01
BOD1L siRNA + Mirin	ND	ND	0.68	0.01

I

siRNA: Control, BOD1L SMARTpool, BOD1L siRNA18, BOD1L siRNA19, BOD1L siRNA20, BOD1L siRNA21
- RAD51
- DAPI

J

| | Con | SP | 18 | 19 | 20 | 21 |
(BOD1L siRNA)
- BOD1L
- RAD51

Figure S6

Figure S7

SUPPLEMENTAL FIGURE LEGENDS

2 **Figure S1: BOD1L ensures cellular viability and genome integrity after replication**

3 **stress. Related to Figure 1. (A)** Total peptides identified by mass spectroscopy analysis of

4 EdU-coprecipitates isolated from HeLa S3 cells. A complete mass spectrometry data set is

5 available on request to the Corresponding Author. **(B)** WCE from parental HeLa or HeLa-

6 CFlap-mBod1L cells (clone 5-20; see also **Figure S2B**) were subjected to IP with anti-GFP

7 antibody, and inputs and recovered immunoprecipitates were analyzed by immunoblotting.

8 Blots originate from a single gel. A white line denotes removal of irrelevant lanes. **(C)** HeLa

9 cells were transfected with the indicated siRNA for 72 h and exposed to the indicated doses of

10 UV-C or aphidicolin (APH), left to form colonies for 14 days, and then stained with methylene

11 blue and counted. **(D)** U-2-OS and H1299 cells were transfected as in (C), exposed to 50
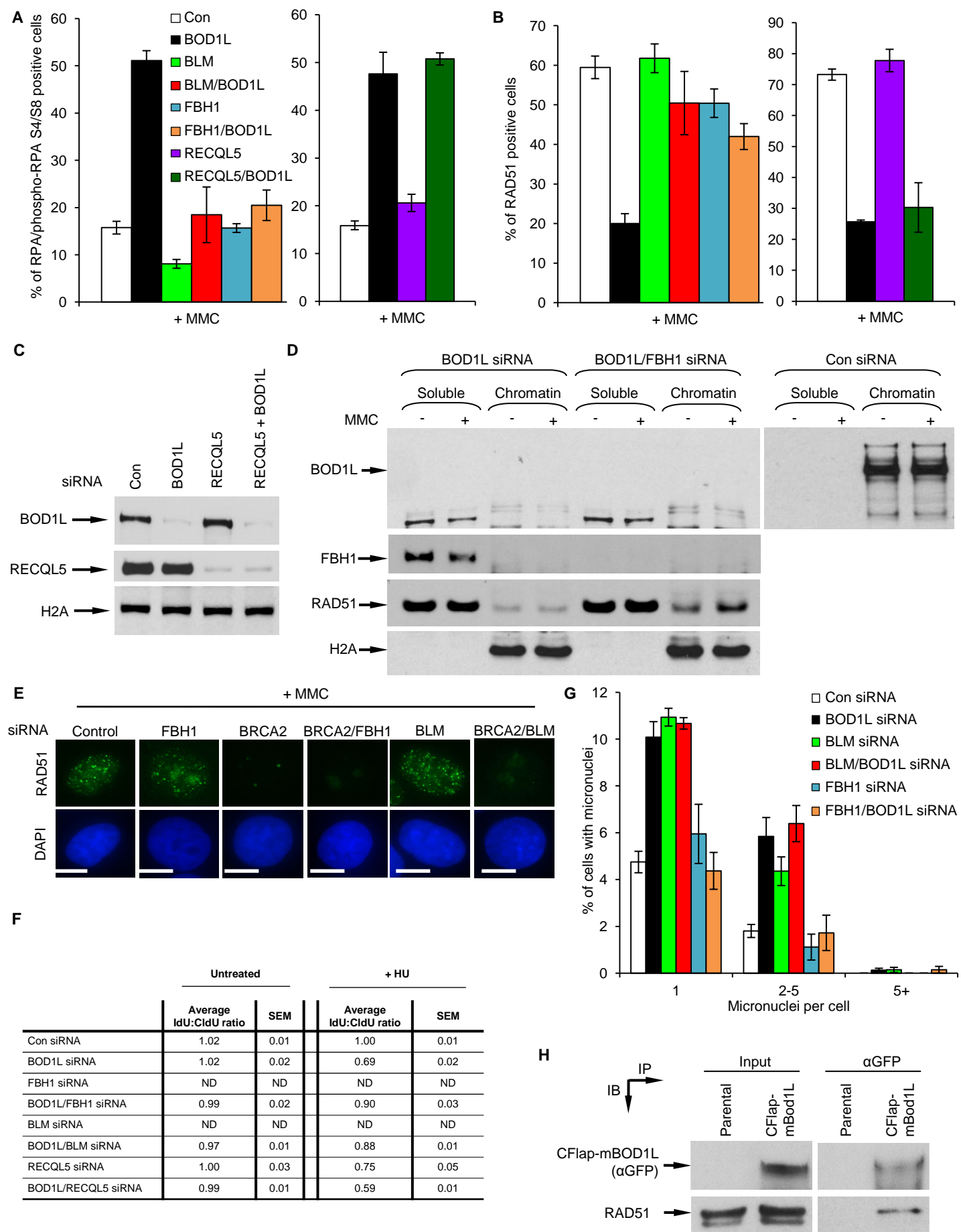
12 ng/ml MMC for 24 h, and micronuclei formation was assessed by immunofluorescence. **(E)**

13 PCR screening of WT and BOD1L-deleted (Δexon 1/Δexon 10) DT40 clones using the primers

14 in (F). The presence of PCR products denotes successful recombination of the homology

15 arms, and thus deletion of the desired region. **(F)** Schematic of the *Gallus gallus* BOD1L locus

16 (*upper*) with targeting vectors spanning exons 1-5 and exon 10 (*middle*), and a schematic of

17 the targeted Δexon 1/Δexon 10 locus (*lower*). Positions of screening primers are shown. **(G)**

18 WT DT40s, and two clones lacking exons 1-5 and exon 10 of BOD1L, were exposed to the

19 indicated doses of MMC, left to form colonies in soft agar, stained with methylene blue and

20 counted. Plots represent mean data from four independent experiments; error bars represent

21 SEM. Two-way ANOVA. **(H)** WT or BOD1L-deleted DT40s were exposed to 12.5 ng/ml MMC

22 for 24 h, and micronuclei formation assessed by immunofluorescence. Plots represent mean

23 data from three independent experiments; error bars represent SEM; Student's t-test. * =

24 $p<0.05$; *** = $p<0.001$.

25

26 **Figure S2: BOD1L knockdown increases genomic instability after replication stress.**

27 **Related to Figure 3. (A)** HeLa, A549 and U-2-OS cells were treated as in **Figure 3G**, and

28 damage to metaphase chromosomes was analysed by Geimsa staining and light microscopy.

29   Graphs integrate data from 50 cells for each condition from three independent experiments.

30   **(B-D)** Parental HeLa or HeLa-CFlap-mBod1L cells (clones C1-4 and C5-20) were transfected

31   with the indicated siRNA for 72 h, and: (B) Whole cell extracts of cells (WCE) were analysed

32   by immunoblotting; (C) Micronuclei formation was assessed by immunofluorescence; (D)

33   Metaphase chromosomes were analysed by Geimsa staining and light microscopy. **(E)** HeLa

34   cells from **Figure 3A** were immunostained with antibodies to FANCD2, and foci formation

35   analysed by fluorescence microscopy. Plot indicates quantification of cells with more than 10

36   FANCD2 foci per cell from four independent experiments. **(F)** U-2-OS cells were transfected

37   with the indicated siRNA for 72 h, exposed to 250 ng/ml MMC for 3 h, left to recover for the

38   indicated times, and WCE were analysed by immunoblotting. Scale bars = 10 μm. NS =

39    $p > 0.05$; ** = $p < 0.01$; Students' t-test.

40

41   **Figure S3: The effect of BOD1L depletion on DNA replication kinetics. Related to Figure**

42   **4. (A)** Quantification of cell cycle profiles shown in **Figure 4B**. Data is representative of the

43   mean ± SEM of four independent experiments. **(B)** Cells from (A) were immunostained with

44   antibodies to phosphorylated histone H3-Ser10, and the percentage of mitotic cells determined

45   by flow cytometry. Data represent mean ± SEM of four independent experiments. **(C)** DNA

46   fibres from **Figure 4E** were quantified. The percentages of ongoing forks, first-label

47   (bidirectional) origins, new origins (IdU-labelled only), first-label terminations (CldU-labelled

48   only) and second label terminations are displayed. **(D)** HeLa cells were treated as in **Figure**

49   **4E** except that, where indicated, they were treated with CDK1/2 inhibitor for 3 h prior to pulse

50   labelling. Plot displays percentage of new origins (IdU-labelled only). **(E)** U-2-OS cells were

51   transfected with the indicated siRNA for 72 h, and DNA fibres prepared as in **Figure 4E**. The

52   percentage of new origins (IdU-labelled only) is displayed. **(F)** HeLa cells were transfected with

53   the indicated siRNAs, and the DNA combed and analysed as above. **(G)** Cells were treated as

54   in **Figure 4D**, except that, where indicated, they were treated with CDK1/2 inhibitor for the

55   duration of HU exposure (2 h). Plots display average percentages of the relevant fork

56   structure(s) from three independent experiments; error bars represent SEM. ** = p<0.01;

57   Students' t-test.

58

59   **Figure S4: BOD1L is necessary to prevent excessive ssDNA formation and RPA2 hyper-**

60   **phosphorylation after replication stress. Related to Figure 5.** **(A)** Foci formation in HeLa

61   cells from **Figure 5B** was analysed by fluorescence microscopy, and fluorescence intensity

62   per nucleus was quantified using ImageJ. Lines denote mean values from three independent

63   experiments. **(B)** U-2-OS cells were treated as in **Figure 5C**, and immunostained with

64   antibodies to BrdU and γH2AX. Representative images are shown. Scale bars = 10 μm. **(C-E)**

65   Vector U-2-OS or SUPER-RPA U-2-OS cells were transfected with the indicated siRNAs and

66   exposed to 50 ng/ml MMC for 24 h. (C) *Left panel*: WCE of the indicated cell lines were

67   analysed by immunoblotting. *Right panel*: Transfected Vector or SUPER-RPA cells were

68   treated as in **Figure 4E**, and the plots display the percentage of new origins (IdU-labelled

69   only). (D) Damage to metaphase chromosomes was analysed by Geimsa staining and light

70   microscopy. Graphs integrate data from 150 cells, in total, for each condition from three

71   independent experiments, and are displayed as fold change compared to control siRNA-

72   transfected cells. (E) WCE of the indicated cell lines were analysed by immunoblotting. **(F)**

73   Parental HeLa or HeLa-CFlap-mBod1L cells (clones C1-4 and C5-20) were transfected with

74   the indicated siRNA for 72 h, exposed to 50 ng/ml MMC for 24 or 48 h, and WCE were

75   analysed by immunoblotting. **(G)** HeLa cells were transfected with the indicated siRNA for 72

76   h, exposed to 250 μM HU for 24 h, and harvested immediately (LI), or left to recover for a

77   further 24 h (WO). WCE were analysed by immunoblotting.

78

79   **Figure S5: BOD1L is required to suppress aberrant end resection at replication forks**

80   **after replication stress. Related to Figure 6.** **(A)** U-2-OS cells were transfected with the

81   indicated siRNAs for 72 h, pulsed for 20 min each with CldU and IdU, and exposed to 4 mM

82   HU for 5 h. DNA was visualised with antibodies to CldU and IdU, and replication fork length

83   was calculated. Plots denote the average ratios of IdU:CldU label lengths from three

84 independent experiments. Arrows indicate mean ratios. (*Inset*) WCE of cells were analysed by

85 immunoblotting. Control siRNA panel is from the same gel as in **Figure S7C**. A white line

86 denotes removal of irrelevant lanes. **(B)** Average values of IdU:CldU label lengths from DNA

87 isolated from cells in **Figures 6A and S6A** is indicated, and SEM are denoted. **(C)** HeLa cells

88 were transfected for 72 h with the indicated siRNAs, exposed to the indicated doses of MMC,

89 left to form colonies for 14 days, and then stained with methylene blue and counted. Plots

90 denote the average values from three independent experiments. **(D)** WCE of cells from (C)

91 were analysed by immunoblotting. Loading control denotes a non-specific protein detected by

92 anti-BOD1L antibody. **(E)** HeLa cells from (C) were exposed to 50 ng/ml MMC for 24 h,

93 immunostained with antibodies to RPA2 and phospho-RPA S4/S8, and foci formation was

94 analysed by fluorescence microscopy. The average percentage of double-positive cells is

95 shown. **(F)** HeLa cells were transfected with the indicated siRNA for 72 h, exposed to 50 ng/ml

96 MMC for 24 h, immunostained with antibodies to RPA2 and phospho-RPA S4/S8, and foci

97 formation was analysed by fluorescence microscopy. The average percentage of double-

98 positive cells from three independent experiments is shown. **(G)** WCE of HeLa cells from (F)

99 were analysed by immunoblotting. **(H)** DNA from U-2-OS cells in **Figure 6C** was visualised

100 with antibodies to CldU and IdU, and replication fork length was calculated. Average values

101 and SEM are denoted. **(I-J)** HeLa cells were transfected with the indicated siRNAs, exposed to

102 50 ng/ml MMC for 24 h, and either: RAD51 foci formation was analysed by fluorescence

103 microscopy (I); or RAD51 expression was analysed by immunoblotting (J). siRNAs18-21 were

104 individual siRNAs from the SMARTpool.

105

106 **Figure S6: BOD1L enables RAD51 chromatin loading to promote efficient homologous**

107 **recombination. Related to Figure 6. (A)** HeLa cells were transfected with the indicated

108 siRNA for 72 h, exposed to 50 ng/ml MMC for 24 h, and immunostained with antibodies to

109 RAD51. Foci formation was analysed by fluorescence microscopy, and quantified into three

110 distinct phenotypes (representative images are shown in the lower panel). **(B-C)** Parental

111 HeLa or HeLa-CFlap-mBod1L cells (clones C1-4 and C5-20) were transfected with the

112   indicated siRNA for 72 h, exposed to 50 ng/ml MMC, and immunostained with antibodies to

113   RAD51. (B) Foci formation was analysed by fluorescence microscopy and quantified. (C)

114   Representative images are shown. **(D)** The incidence of radial chromosome formation was

115   analysed from metaphase spreads prepared as described in **Figure 3G**. ** = p<0.01; Students'

116   t-test. **(E)** HeLa cells were transfected with the indicated siRNA for 24 h, labelled with BrdU for

117   a further 24 h, and exposed to 25 ng/ml MMC for a further 24 h. Sister chromatid exchanges

118   were quantified from at least 50 cells from three independent metaphase spreads. Line =

119   mean number of SCEs/chromosome. Error bars = SEM. *** = p<0.001; Mann-Whitney ranked

120   sum test. **(F)** HeLa cells were transfected with the indicated siRNA for 72 h, exposed to 5 Gy

121   of γ-irradiation, and immunostained with antibodies to RAD51. Scale bars = 10 μm. **(G-I)** The

122   prevalence of nuclear foci of BRCA1, BRCA2, and PALB2-GFP in HeLa or U-2-OS-PALB2-

123   GFP cells from **Figure 6H**. Foci formation was analysed by fluorescence microscopy, and

124   representative images are shown.

125

126   **Figure S7: BOD1L acts to restrain anti-recombinase activity to stabilise RAD51**

127   **chromatin loading and prevent excessive resection of replication forks. Related to**

128   **Figure 7. (A-B)** HeLa cells were treated as in **Figure 7A/B**, and RPA2/RPA2-PS4/8 foci

129   formation (A) or RAD51 foci formation (B) was analysed by fluorescence microscopy. The

130   average percentage of double-positive cells (A) or RAD51-positive cells (B) is shown. **(C)**

131   WCE of cells from (A) were analysed by immunoblotting. **(D)** U-2-OS cells were transfected

132   with the indicated siRNAs, exposed to 100 ng/ml MMC for 24 h, and then fractionated. Soluble

133   and chromatin fractions were analysed by immunoblotting. Blots originate from a single gel. A

134   white line denotes removal of irrelevant lanes. **(E)** HeLa cells were transfected with the

135   indicated siRNA for 72 h, exposed to 50 ng/ml MMC for 24h, and immunostained with

136   antibodies to RAD51. Scale bars = 10 μm. **(F)** U-2-OS cells were treated as in **Figure 7C**, and

137   IdU:CldU ratios were calculated in the presence/absence of HU. Average values and SEM are

138   denoted. **(G)** Micronuclei formation was assessed by immunofluorescence in HeLa cells from

139   **Figure 7A**. **(H)** WCE from parental HeLa or HeLa-CFlap-mBod1L cells from **Figure S1B** were

140   subjected to IP with anti-GFP antibody, and inputs and recovered immunoprecipitates were

141   analyzed by immunoblotting. The upper panel is identical to that shown in **Figure S1B**. A white

142   line denotes removal of irrelevant lanes.

143 **SUPPLEMENTAL EXPERIMENTAL PROCEDURES**

144 **Cell lines**

145 A549, HeLa, HeLa S3, U-2-OS, and H1299 were sourced from the ATCC. U2OS-PALB2-GFP

146 were obtained from F. Esashi. HeLa-FUCCI were obtained from RIKEN BRC.

147

148 **Drugs and inhibitors**

149 HU, Aphidicolin, and MMC were from Sigma Aldrich, and were used as indicated in the Figure

150 Legends. Cdk1/2 inhibitor III was used at 25 µM (Merck). dNTP analogues BrdU, EdU, CldU

151 and IdU were from Sigma Aldrich, and were used as indicated. Mirin (Calbiochem) was used

152 at 50 µM.

153

154 **Generation of HeLa-CFlap-BOD1L cells.**

155 A BAC containing the full length *Mus musculus* BOD1L locus was obtained from BacPac

156 Resources. This BAC was modified to insert a C-terminal Flap tag by Red/ET recombination

157 following a modified protocol from Genebridges. To generate HeLa-CFlap-BOD1L cells, HeLa

158 cells have been transfected with CFlap-Bod1L BAC using Lipofectamine 2000 (Invitrogen),

159 then selected for 3 weeks with Geneticin and single cell-sorted by FACS following high level of

160 GFP expression. Two clones (C1-4 and C5-20) were expanded and used for further

161 experiments.

162

163 **Generation of BOD1L knock out DT40 cell lines.**

164 BOD1L knock out DT40 cell lines were generated using two disruption cassettes targeting

165 exons 1-5 and targeting exon 10 of the chicken BOD1L locus. The chicken BOD1L locus was

166 identified by BLAST search using the human protein sequence against the ENSEMBL draft

167 chicken genome sequence. An ENSEMBL predicted transcript encompassed the entire

168 BOD1L gene. From this sequence, two disruption cassettes targeting exons 1-5 and targeting

169 exon 10 were designed. PCR oligos used to amplify 5′ and 3′ arms of the first construct

170 targeting   exons   1-5   were

171   GCGGCCGCGGTCTCGGATCCATGGAGCGACAATGATGACACAGATGG/

172   GGTGATATCGGCGGCAAGCTGGCTACAGCGTGTTAGGAGGGTTGAGTG   and

173   ATTATACGAACGGTACTCGATGATTTGAAGAGGAAAGTGAAGAAGAACCTGTG/

174   GGATCCGAGACCGCGGCCGCCCTATCTTACTCACCACCCCCAAGTCCTCA   respectively.

175   PCR oligos used to amplify 5′ and 3′ arms of the second construct targeting exon 10 were

176   AATATAAAGCTTGCGGCCGCCAGCGTTGTCCAAAGGACATCTG/

177   GTCAAGCTTCTATTTGGCATCTGTGGCTTGGACTG   and

178   GTACTTGAGTAGCGTGTAATCAGTGCAAGTGCTGATG/

179   GGCAAGCTTATAGCAGGGTGGGTTGGAACTAGATG respectively.   Targeting constructs

180   were generated by cloning the PCR products into the pSH vector containing either puromycin

181   or hygromycin resistance. Transfections and selection of targeted DT40 clones were carried

182   out as described previously (Niedzwiedz *et al*., 2004). To confirm the appropriate disruptions

183   of the GgBOD1L locus, genomic DNA was obtained and the following PCR oligos were used

184   to   screen   the   clones: ScrF1,   TGCATCAGGGATGCACATTCTC;   ScrR1,

185   TAAGACTGCTGCTGACACCTTCAC;   ScrF2,   GCGGGACTATGGTTGCTGACTAATTGAG;

186   ScrR2,   ACTAGCTGCGTCCCAAAGAGTTTC;   ScrF3,

187   GCTGGCATGCTGGAATGTACTTTATGG;   ScrR3,

188   CTTCACAGAGGCGAGTAACTTCCTGTAAC;   ScrF4,

189   ACGATTCCGAAGCCCAACCTTTCATAG; ScrR4, ATCTTTGGAGATGTTCAAGGCCAGGTC

190   (**Figure S1E**).

191

192   **siRNA Transfections**

193   siRNAs were from Dharmacon as SMARTpool (SP) or individual siRNAs deconvolved from the

194   SMARTpool: BOD1L (SP, siRNA-18,-19,-20,-21); BOD1 (SP). SP and BOD1L siRNA-19 were

195   used for all experiments unless stated. siRNA transfections were performed with siRNA

196   duplexes (100 nM) using Oligofectamine (Invitrogen). Whenever siRNAs were combined, the

197   total   concentration   was   kept   at   100   nM.   A   custom   siRNA   targeting   lacZ

198   (CGUACGCGGAAUACUUCGAdTdT) was used as a scrambled, non-targeting siRNA, and is

199   abbreviated as "Control siRNA", or "Con siRNA". All experiments were performed 72 h post

200   knockdown unless otherwise stated.

201

202   **Colony survival assays**

203   Colony survival assays using HeLa cells were carried out as described (Stewart *et al.*, 2003).

204   For colony survival assays with DT40 cells, MMC-treated cells were plated in methylcellulose

205   after exposure to a range of concentrations of the drug. Viable colonies were scored after 2-3

206   weeks.

207

208   **DNA combing**

209   DNA combing was carried out essentially as described previously (Petermann *et al.*, 2010).

210   HU (2 mM) or MMC (50 ng/ml) treatments were for 2 h or 24 h respectively. For resection

211   experiments, cells were pulse-labelled with CldU and IdU for 20 min each before a 5 h

212   exposure to 4 mM HU. For quantification of replication structures, at least 250 structures were

213   counted per experiment. The lengths of red or green labelled tracts were measured using

214   ImageJ (National Institutes of Health; http://rsbweb.nih.gov/ij/) and arbitrary length values were

215   converted into micrometers using the scale bars created by the microscope.

216

217   **Chromatin fractionation**

218   Subcellular fractionations were performed in U-2-OS cells essentially as described in (Mendez

219   and Stillman, 2000), except that chromatin fractions were washed once after isolation in 200

220   mM NaCl, 3 mM EDTA, 0.2 mM EGTA, 1 mM DTT, plus protease inhibitor cocktail, and re-

221   suspended in UTB.

222

223   **Metaphase spreads, SCEs and FISH**

224   Chromosomal aberrations and sister chromatid exchanges (SCEs) were scored in Giemsa

225   stained metaphase spreads. For chromosome aberrations, demecolcine (Sigma) was added

226   3-4 h prior to harvesting at a final concentration of 0.2 µg/ml. Cells were harvested by

227 trypsinisation, subjected to hypotonic shock for 1 hour at 37°C in 0.3 M sodium citrate and

228 fixed in 3:1 methanol:acetic acid solution. Cells were dropped onto acetic acid humidified

229 slides, stained for 15 minutes in Giemsa-modified (Sigma) solution (5% v/v in H2O) and

230 washed in water for 5 minutes.

231

232 For SCEs, 10 µM BrdU (Sigma) was added to the medium for two complete cycles

233 (approximately 48 hours) before collection and 25ng/ml MMC was added 24 h before

234 collection. 0.2 µg/ml demecolcine was added 3 h prior to harvesting and metaphase spreads

235 were obtained as described above. Before Giemsa staining, slides were incubated in Hoescht

236 33258 solution (10 µg/ml) for 20 minutes, exposed to UV light (355 nm) for 1 hour and washed

237 for 1 hour at 60°C in 20× SCC. Cells were harvested as described above.

238

239 Fragile site FISH was performed as previously described by (Le Tallec *et al*., 2011). Probes

240 for the common fragile sites FRA3B and FRA16D were made from BACs RP11-170K19 and

241 RP11-281J9, respectively (Children's Hospital Oakland Research Institute) and were labelled

242 with Biotin-conjugated nucleotides using the BIOPRIME DNA Labelling System (Invitrogen)

243 according to manufacturer's protocol. For dioxigenin incorporation, the BIOPRIME DNA

244 Labelling System was used, but Dioxigenin-conjugated dNTPs (Roche) were used instead of

245 biotin-conjugated dNTPs. Probes were purified using Illustra Probequant G-50 micro columns

246 (GE Healthcare).

247

248 **Flow cytometry**

249 Flow cytometry was carried out as described previously (Townsend *et al*., 2009). Briefly, HeLa

250 cells were harvested, fixed in 70% ethanol at -20°C for at least 1 h, and permeabilised with

251 0.25% Triton-X100 for 15 at 4°C. For immuno-detection of phospho-histone H3 (Ser10), cells

252 were then incubated with primary antibody for 1 h, washed in 1% BSA, and counterstained

253 with Alexa Fluor-488 goat anti-mouse IgG antibody. Cells were then washed twice with 1%

254 BSA, and stained with 25 µg/ml propidium iodide containing 0.1 mg/ml RNase A. Cells were

255 analysed using an Accuri flow cytometer (BDBiosciences) in conjunction with CFlowplus

256 software. Data represents that obtained from at least 30,000 cells.

257

258 **Antibodies and Western blotting**

259 Whole cell extracts were obtained by sonication in UTB buffer (8 M Urea, 50 mM Tris, 150 mM

260 β-mercaptoethanol, protease inhibitor cocktail (Roche)) and analysed by SDS-PAGE following

261 standard procedures. The following antibodies were used: H2A, γ-H2AX, BRCA2, RPA2,

262 RAD51 (Merck Millipore); MRE11, phospho-histone H3 Ser-10, phospho-CDK2 Tyr-15 (Cell

263 Signalling); MCM7, CHK1, PCNA, CDK2, FANCD2, BRCA1, BRCA2 (Santa Cruz

264 Biotechnology); RECQL5, FANCA, EXO1, phospho-RPA2 Ser-4/8, phospho-CHK1 Ser-317,

265 phospho-CHK1 Ser-345, MLL1 (Bethyl); CENPA, DNA2, BOD1, PCNT-1 (Abcam), α-tubulin,

266 FLAG (Sigma Aldrich); GFP (Roche); BrdU (CldU) (AbD Serotec); BrdU (IdU) (Becton

267 Dickinson); MCM2 (BD Transduction); 53BP1 (G. S. Stewart); PICH (H. Yu). Affinity purified

268 polyclonal anti-BOD1L antibodies were generated by immunising rabbits with a purified GST-

269 fusion protein spanning amino acids 1,900 to 2,501 of human BOD1L (Accession number:

270 NP_683692.2) (Eurogentec).

271

272 **Immunoprecipitations**

273 HeLa nuclear cells extracts (Cilbiotech) were clarified by centrifugation at 44,000 x g,

274 immunoprecipitated with 5 µg of anti-BOD1L antibody or IgG for 3 h at 4 °C. After further

275 clarification, immune complexes were isolated using protein-A sepharose (GE Healthcare),

276 and analysed by immunoblotting.

277

278 **iPOND**

279 *EdU-labeled sample preparation*: Logarithmically growing HeLa S3 cells (1×10^6 per ml) were

280 incubated with 10 mM EdU for 10 min. Following EdU labelling, cells were fixed in 1 %

281 formaldehyde, quenched by adding glycine to a final concentration of 0.125 M and washed in

282 PBS three times. Collected cell pellets were frozen at -80 °C and cells were permeabilised by

283   resuspending in ice cold 0.25 % Triton-X/PBS at a concentration of 1-1.5 x 10^7 cells per ml

284   and incubating on ice for 30 min. Before the Click reaction, samples were washed once in 0.5

285   % BSA/PBS and once in PBS.

286

287   *Click reaction*: Cells were incubated in Click reaction buffer for 1h at room temperature

288   containing 10 µM azide-PEG(3+3)-S-S-biotin conjugate (Click ChemistryTools, cat. no AZ112-

289   25), 10 mM sodium ascorbate, and 1 mM copper (II) sulfate (CuSO4) in PBS. The 'no Click'

290   reaction contained DMSO instead of biotin-azide. Following the Click reaction, cells were

291   washed once in 0.5 % BSA/PBS and once in PBS. Cells were resuspended in lysis buffer (50

292   mM Tris–HCl pH 8.0, 1 % SDS) containing protease inhibitor cocktail (Roche) and sonicated

293   using a Diagenode Bioruptor® Plus for 40 cycles (30 sec on/30 sec off). Samples were

294   centrifuged at 14,500 xg at 4°C for 30 min and the supernatant was diluted 1:3 with NTN buffer

295   (100 mM NaCl, 20 mM Tris pH 7.4 and 0.05 % NP40) containing protease inhibitors. An

296   aliquot was taken as an input sample.

297

298   *Purification*: Streptavidin–agarose beads (Novagen) were washed three times in NTN buffer

299   containing protease inhibitor cocktail. 200 µl of bead slurry was used per 1x 10^8 cells. The

300   streptavidin–agarose beads were resuspended 1:1 in NTN buffer containing protease

301   inhibitors and added to the samples. Samples were then incubated at 4 °C for 4 h in light

302   exclusion. Following binding, the beads were then washed 4x with 1 ml NTN buffer and

303   protein-DNA complexes were eluted by incubating with 5mM DTT in NTN buffer. Cross-links

304   were reversed by incubated samples in SDS sample buffer at 95 °C for 12 min. Proteins were

305   resolved on SDS-PAGE and detected by immunoblotting, or mass-spectrometry analysis was

306   performed on the eluates. Mass spectrometry was carried out as described previously

307   (Adelman *et al.*, 2013). A complete mass spectrometry data set is available on request to the

308   Corresponding Author.

309

310

Microscopy and Image Analysis

HeLa, H1299, U-2-OS, HeLa-FUCCI or A549 cells were grown on glass coverslips. DT40 cells were grown in suspension, and dropped onto poly-L-lysine coated coverslip for 15 min. Cells were washed with PBS twice before fixation. For α-tubulin, PCNT-1, PCNA, CENPA and 53BP1 immuno-detection, cells were fixed with methanol at -20 °C for 10 minutes. For PICH, FANCD2 and EdU detection, and for 53BP1 immuno-detection in FUCCI cells, cells were fixed in 3.6% paraformaldehyde for 10 min at room temperature before permeabilisation with nuclear extraction buffer (10 mM PIPES, 20 mM NaCl, 3 mM $MgCl_2$, 300 mM sucrose, 0.5% Triton X-100) for 10 minutes. For RAD51, γ-H2AX, BRCA2 and RPA immuno-detection, cells were pre-treated with nuclear extraction buffer for 5 minutes on ice, and fixed in 3.6% paraformaldehyde for 10 minutes at room temperature. For in situ detection of nascent DNA in mitotic and interphase cells the Click-iT DNA Alexa Fluor 495 Imaging Kit (Invitrogen) was used. For ssDNA (BrdU) analyses, cells were pre-treated with nuclear extraction buffer for two 5 consecutive minute incubations on ice, then fixed as above. After fixation, cells were washed with PBS three times and then blocked with ADB (Antibody Dilution Buffer; 5% FCS in PBS) for 1 h at 4°C. Cells were incubated with primary antibody (diluted in ADB) for 1 h at room temperature, washed with ADB and then counterstained with Alexa Fluor-488 goat anti-rabbit IgG, Alexa Fluor-594 goat anti-mouse IgG, Alexa Fluor-350 goat anti-rabbit IgG, or Alexa Fluor-555 donkey anti-rabbit IgG secondary antibodies (Molecular Probes) diluted in ADB, for 1 h at room temperature. Cells were then washed twice with ADB and coverslips were mounted onto glass slides with Vectashield mounting agent containing 0.4 µg/ml DAPI (Vectashield). Fluorescence images were taken using a Nikon E600 Eclipse microscope equipped with a 60X oil lens, and images were acquired and analysed using Volocity Software v4.1 (Improvision). For ssDNA analyses, BrdU foci were enhanced using the ImageJ convolve function, and the number of nuclear foci/cell quantified.

Proximity ligation assays

338   For proximity ligation assays (PLA), cells were fixed/permeabilised as appropriate for the

339   primary antibodies used, incubated in primary antibody, and in situ proximity ligation was

340   performed using Duolink Detection Kit in combination with anti-Mouse PLUS and anti-Rabbit

341   MINUS PLA Probes, according to the manufacturer's instructions (Sigma Aldrich Duolink).

342   Nuclear foci were imaged as above, and the number of nuclear foci/cell quantified using

343   ImageJ.

344 **SUPPLEMENTAL REFERENCES**

345

346 Adelman, C.A., Lolo, R.L., Birkbak, N.J., Murina, O., Matsuzaki, K., Horejsi, Z., Parmar, K.,

347 Borel, V., Skehel, J.M., Stamp, G., et al. (2013). HELQ promotes RAD51 paralogue-dependent

348 repair to avert germ cell loss and tumorigenesis. Nature 502, 381-384.

349

350 Le Tallec, B., Dutrillaux, B., Lachages, A.M., Millot, G.A., Brison, O., and Debatisse, M. (2011).

351 Molecular profiling of common fragile sites in human fibroblasts. Nature structural & molecular

352 biology 18, 1421-1423.

353

354 Mendez, J., and Stillman, B. (2000). Chromatin association of human origin recognition

355 complex, cdc6, and minichromosome maintenance proteins during the cell cycle: assembly of

356 prereplication complexes in late mitosis. Molecular and cellular biology 20, 8602-8612.

357

358 Niedzwiedz, W., Mosedale, G., Johnson, M., Ong, C.Y., Pace, P., and Patel, K.J. (2004). The

359 Fanconi anaemia gene FANCC promotes homologous recombination and error-prone DNA

360 repair. Molecular cell 15, 607-620.

361

362 Townsend, K., Mason, H., Blackford, A.N., Miller, E.S., Chapman, J.R., Sedgwick, G.G.,

363 Barone, G., Turnell, A.S., and Stewart, G.S. (2009). Mediator of DNA damage checkpoint 1

364 (MDC1) regulates mitotic progression. The Journal of biological chemistry 284, 33939-33948.

365

366 Stewart, G.S., Wang, B., Bignell, C.R., Taylor, A.M., and Elledge, S.J. (2003). MDC1 is a

367 mediator of the mammalian DNA damage checkpoint. Nature *421*, 961-966.